

VitalBench: A Rigorous Multi-Center Benchmark for Long-Term Vital Sign Prediction in Intraoperative Care

Xiuding Cai, Xueyao Wang, Sen Wang, Yaoyao Zhu, Jiao Chen and Yu Yao

Abstract—Intraoperative monitoring and prediction of vital signs are critical for ensuring patient safety and improving surgical outcomes. Despite recent advances in deep learning models for medical time-series forecasting, several challenges persist, including the lack of standardized benchmarks, incomplete data, and limited cross-center validation. To address these challenges, we introduce VitalBench, a novel benchmark specifically designed for intraoperative vital sign prediction. VitalBench includes data from over 4,000 surgeries across two independent medical centers, offering three evaluation tracks: complete data, incomplete data, and cross-center generalization. This framework reflects the real-world complexities of clinical practice, minimizing reliance on extensive preprocessing and incorporating masked loss techniques for robust and unbiased model evaluation. By providing a standardized and unified platform for model development and comparison, VitalBench enables researchers to focus on architectural innovation while ensuring consistency in data handling. This work lays the foundation for advancing predictive models for intraoperative vital sign forecasting, ensuring that these models are not only accurate but also robust and adaptable across diverse clinical environments. Our code and data are available at https://github.com/XiudingCai/ VitalBench.

Index Terms—Vital Sign Prediction, Intraoperative Monitoring, Multivariate Time-Series Forecasting.

I. INTRODUCTION

NTRAOPERATIVE monitoring and prediction of vital signs, such as heart rate, blood pressure, and oxygen saturation, are critical for ensuring patient safety and optimizing surgical outcomes [1]–[4]. These physiological indicators provide real-time insight into a patient's physiological state and enable

This work was supported in part by the Sichuan Provincial Science and Technology Department under Grant 2022YFS0384 and 2022YFQ0108, and in part by the Chengdu Science and Technology Program under Grant 2022-YF04-00078-JH. (Corresponding authors: Jiao Chen and Yu Yao.)

Xiuding Cai, Xueyao Wang, Sen Wang, Yaoyao Zhu and Yu Yao are with Chengdu Institute of Computer Application, Chinese Academy of Sciences, Chengdu, China, and with the School of Computer Science and Technology, University of Chinese Academy of Sciences, Beijing, China (e-mail: {caixiuding20, wangxueyao221}@mails.ucas.ac.cn, casitmed2022@163.com).

Sen Wang was with Digital Intelligent Technology Branch, Southwest Oil & Gas Field, PetroChina (e-mail: wangsen05@petrochina.com.cn).

Yaoyao Zhu was with China Zhenhua Research Institute Co., Ltd., Guiyang, China (e-mail: zhuyaoyao19@mails.ucas.ac.cn).

Jiao Chen was with Department of Anesthesiology, West China Hospital, Sichuan University & The Research Units of West China (2018RU012) (e-mail: chenjiao@wchscu.cn).

early detection of potential complications. Accurate forecasting of vital sign trend allows surgical teams to anticipate risks and implement timely interventions, thereby reducing adverse events and improving postoperative recovery [5]–[8].

Recent advances in deep learning [9]–[13], particularly in managing complex, multivariate time-series data, have shown considerable promise in medical data analysis, pattern recognition, and improving predictive accuracy. Models such as Recurrent Neural Networks (RNNs) [14]–[16], Convolutional Neural Networks (CNNs) [17]–[19], Multi-Layer Perceptrons (MLPs) [20], [21], Graph Neural Networks (GNNs) [22], [23] and Transformers [24]–[27] have achieved notable success across a range of healthcare applications, providing novel methodologies for vital sign prediction. These approaches are capable of identifying latent patterns within large-scale medical datasets, thereby significantly enhancing the precision and reliability of clinical predictions.

Despite the promising results of deep learning in vital sign prediction, several challenges persist:

Challenge 1: Lack of Standardized Benchmarks and Inconsistent Preprocessing. The field of vital sign prediction is characterized by a fragmented landscape where studies often rely on proprietary datasets and diverse preprocessing pipelines [28], [29]. This fragmentation not only obstructs direct model comparisons but also undermines reproducibility. Without a unified benchmark, the community faces difficulties in identifying fundamental improvements or addressing gaps across different approaches, stalling collective advancements.

Challenge 2: Assumption of Complete Data Availability. Many existing studies implicitly assume complete vital sign data [30], [31], where all monitoring variables are consistently available for each patient. In practice, however, sensor failures, detachment events, and individualized monitoring setups result in frequent and structured missingness. Models trained under this assumption often degrade in performance when facing incomplete inputs, emphasizing the need for methods that explicitly accommodate heterogeneous data availability.

Challenge 3: Single-Center Validation. Predominantly, current studies rely on data from a single medical center [32], [33]. However, variability in patient demographics, sensor devices, and clinical protocols across institutions creates a fundamental barrier to real-world applicability. Without crosscenter validation, the robustness and transferability of these models remain untested, raising concerns about their reliability and generalizability in broader clinical deployment.

To tackle these challenges, we propose VitalBench, a comprehensive, clinically grounded benchmark for long-term intraoperative vital sign forecasting. VitalBench comprises data from 4,183 surgeries collected across two medical centers, with 962 from VitalDB [34] and 3,221 from MOVER-SIS [35]. To promote progress in addressing real-world challenges, VitalBench introduces three targeted evaluation tracks:

Track 1: Complete Variables Data. An idealized track where all vital sign variables are fully observed. To preserve clinical realism, raw data are used without imputation, as synthetic filling may distort physiological dynamics. Masked loss functions mitigate the impact of missing values, enabling fair and robust model comparison under consistent conditions.

Track 2: Incomplete Variables Data. A clinically grounded setting where subsets of vital sign variables are missing due to sensor dropout or case-specific configurations. This track challenges models to handle variable missingness and promotes the development of architectures inherently robust to incomplete heterogeneous inputs.

Track 3: Cross-Center Generalization. A transferability evaluation across institutions, where models trained on one medical center are tested on another. It examines robustness to distributional shifts caused by differences in patient populations, monitoring devices, and surgical protocols, encouraging generalizable and deployable forecasting solutions.

Using VitalBench, we conduct a systematic evaluation of a wide range of state-of-the-art time-series forecasting models, including RNNs, CNNs, MLPs, GNNs, and Transformers. The results yield several key insights into the core challenges and design principles of intraoperative vital sign prediction:

- Modeling inter-variable dependencies is crucial for reliable forecasting. Architectures that explicitly mix variables consistently outperform variable-independent ones, particularly under incomplete inputs or heterogeneous data. This reflects the physiological coupling of vital signs and underscores the need to capture crossvariable dynamics for robust and scalable modeling.
- 2) Modeling missingness directly outperforms imputation. models trained with proposed masked loss outperform those using conventional imputation, highlighting the value of preserving the natural missingness patterns in clinical data rather than introducing potentially spurious or temporally inconsistent values that could mislead predictions and reduce clinical reliability.
- 3) Data scale enhances generalization, yet cross-center gaps persist. Training on larger datasets consistently enhances performance, and in some prediction horizons, models trained on large cohorts match results on smaller cohorts, indicating feasible cross-domain transfer. Yet, performance drops remain across centers in most conditions, highlighting the clinical generalization challenge.

Our main contributions are as follows:

We introduce VitalBench, the first multi-center benchmark for long-term intraoperative vital sign forecasting, with three clinically relevant tracks—complete data, incomplete data, and cross-center generalization—designed to evaluate model performance and generalization under real-world surgical conditions.

- 2) We design an end-to-end evaluation framework that reflects real-world clinical challenges, minimizing reliance on heavy preprocessing and employing masked loss to handle missing data, thereby ensuring consistent, reproducible, and fair model comparisons.
- 3) Using VitalBench, we conduct a comprehensive empirical study uncovering key insights for vital sign forecasting, highlighting the need for models that capture inter-variable dependencies, handle variable channel dimensions, and generalize across clinical centers.

II. RELATED WORK

A. Time Series Forecasting

Time series forecasting has progressed from classical statistical methods [39] to deep learning techniques capable of capturing complex temporal dependencies [20], [24], [40]–[43], driven by the growth of large-scale datasets and the demand for models handling intricate patterns.

RNNs [14]–[16] pioneered long-term sequence forecasting (LTSF) by modeling sequential dependencies. Temporal Convolutional Networks (TCNs) [17], [18] emerged as an alternative, effectively capturing local temporal patterns with their localized receptive fields, whileCollectively, these benchmarks enhance reproducibility in ICU research yet fall short of capturing the real-time, high-frequency, and multi-center nature of intraoperative vital-sign prediction. Multi-Scale Isometric Convolution Network (MICN) extended temporal modeling by integrating local and global dependencies across scales, enhancing performance in diverse tasks [19].

Transformers [44], initially designed for natural language processing, have gained prominence in time series forecasting due to their self-attention mechanism, which excels at capturing long-range dependencies [24], [25], [45]. However, the quadratic complexity of self-attention remains a computational bottleneck. Recent innovations, such as patch-based approaches like PatchTST [40], address this limitation, making Transformers more practical for large-scale applications [46].

MLPs, have also shown promise in time series tasks, offering simplicity and efficiency in specific scenarios [20], [21]. GNNs [47], like MTGNN [22], have been particularly effective in multivariate time series, combining graph convolutional and temporal layers to model spatial-temporal relationships. FourierGNN [23] further explores this domain by treating the entire time series as a hypervariate graph and leveraging Fourier transforms for global dependency modeling.

Recently, state-space models [48]–[51] have been introduced to time series forecasting, offering a fresh perspective. For instance, MambaTS [41] achieves linear complexity while effectively modeling global dependencies, demonstrating superior performance compared to Transformer-based methods.

B. Perioperative Time Series Forecasting

Recent years have seen notable progress in applying deep learning to intraoperative vital sign forecasting. Lee et al. [28] developed a long short-term memory (LSTM) model to predict the bispectral index during total intravenous anesthesia using drug infusion histories and demographic features. He et al. [31]

	Dataset	Domain	Frequency	Lengths	Variables	Volume	#Instance	MC
	Exchange [16]	Exchange	1 day	7,588	8	623 KB	1	
	Electricity [36]	Electricity	1 hour	26,304	321	92 MB	1	
	ETTm2 [24]	Electricity	15 mins	57,600	7	9.3 MB	1	
	Traffic [37]	Traffic	1 hour	17,544	862	131 MB	1	
	Solar [16]	Weather	10 mins	52,560	137	8.3 MB	1	
	Weather [37]	Weather	10 mins	52,696	21	7.0 MB	1	
	ILI [37]	Health	1 day	966	7	67.6 KB	1	
	Covid-19 [38]	Health	1 day	1,392	948	5.0 MB	1	
i	VitalBench (Ours)					488.7 MB	4,183	√
	VitalDB	Health	5 secs	2,697,323	17	458.0 MB	962	
	MOVER	Health	1 min	817,161	33	130.7 MB	3,221	

TABLE I: Summary of statistics for different time-series datasets. #Instance represents the number of instances, and MC denotes whether the dataset is multi-center.

further enhanced this framework by combining an LSTM with a gated residual network (GRN) for improved feature extraction. Bahador et al. [30] applied deep learning to EEG-based depth-of-anesthesia estimation, demonstrating the capacity of neural models to capture complex physiological dynamics.

Despite recent progress, existing research remains fragmented and limited. Many studies rely on proprietary datasets or closed-source implementations, impeding reproducibility and external validation. Even public datasets suffer from heterogeneous preprocessing and task definitions, hindering consistent evaluation. Most efforts focus on short-term or single-variable predictions within single-center cohorts, overlooking long-term dependencies, inter-variable correlations, and cross-hospital generalization. As a result, the field lacks a standardized, openly accessible benchmark for fair, reproducible, and clinically relevant assessment of forecasting models.

C. Benchmarks

Benchmarks drive scientific progress by offering standardized datasets, metrics, and protocols for fair and reproducible model comparison [52], [53]. LTSF benchmarks such as Libra [54], TSLib [18], and TFB [55] facilitate cross-domain evaluation and promote methodological advances through unified training and validation protocols.

Medical forecasting, however, faces additional complexities beyond temporal generalization. Clinical data are heterogeneous, sporadic, noisy, and patient-dependent, collected from multiple devices under dynamic physiological and treatment conditions. Consequently, medical benchmarks must address missingness, label imbalance, and inter-patient variability, which are rarely emphasized in standard LTSF frameworks.

Several works have standardized clinical time-series evaluation. Harutyunyan et al. [56] proposed four MIMIC-III [57] benchmarks for mortality, length-of-stay, physiologic decline, and phenotype classification, exploring multitask learning and deep supervision. HiRID [32] provides high-resolution ICU data with structured tasks but sparse interventions and gradually evolving trajectories. Van De Water et al. [58] introduced YAIB, supporting multiple ICU datasets and predefined tasks including mortality, sepsis, and kidney function, yet still focusing on long-term or static outcomes. Clairvoyance [11]

provides a unified pipeline for clinical time-series modeling and evaluation, not designed for vital-sign forecasting. Collectively, these benchmarks enhance reproducibility in ICU research yet fall short of capturing the real-time, high-frequency, and multi-center nature of intraoperative vital-sign prediction.

Intraoperative vital-sign forecasting presents distinct challenges. Signals are recorded at sub-minute resolution under rapidly changing physiological states and frequent interventions, leading to artifacts, missingness, and strong nonstationarity across patients and procedures. Moreover, multi-center validation remains limited [32], [33], despite its importance for generalization across populations and sites. Patient-level data splits are also crucial to prevent leakage and capture inter-patient variability. These gaps highlight the need for a dedicated benchmark for real-time intraoperative forecasting.

Table I summarizes existing time series datasets and introduces our proposed benchmark, VitalBench, specifically designed to address these limitations, providing a foundation for robust and generalizable perioperative vital-sign prediction.

III. VITALBENCH

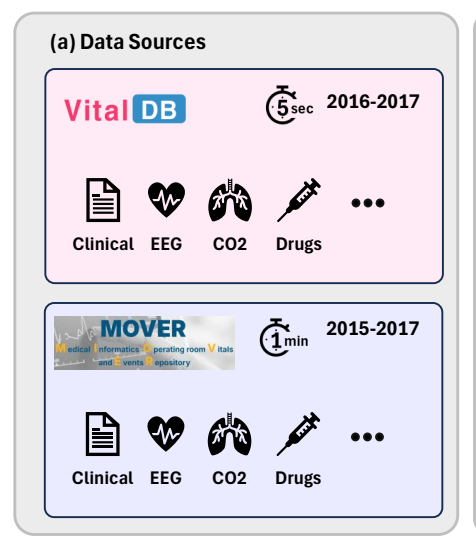
A. Task Description

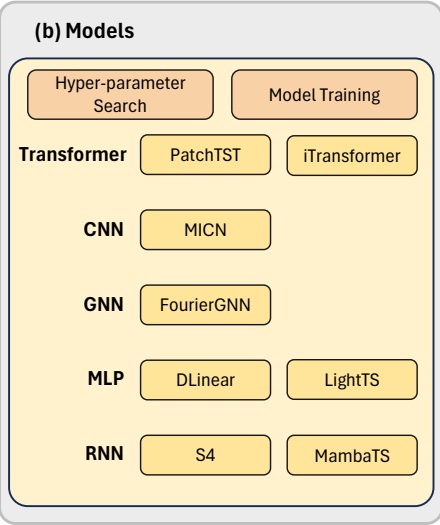
We consider the problem of multivariate time series fore-casting in the operating room. Given a retrospective window $\mathbf{x} = \mathbf{x}_1, \mathbf{x}_2, \cdots, \mathbf{x}_L$ of length L with K variables, where $\mathbf{x}_t \in \mathbb{R}^K$ represents the values of the K variables at time step t, the goal is to predict the values for the next T time steps, denoted as $\mathbf{y} = \mathbf{x}_{L+1}, \mathbf{x}_{L+2}, \cdots, \mathbf{x}_{L+T}$.

In this formulation, the K variables include both static covariates, such as patient demographics and procedure type, and dynamic variables, such as heart rate and blood pressure, which evolve over time. The forecasting task focuses exclusively on predicting the future values of the dynamic variables, while static covariates serve as conditioning context throughout the prediction horizon.

B. Data Collection

VitaIDB Dataset. VitaIDB [34] is a publicly available, high-resolution perioperative dataset from Seoul National University Hospital, comprising 6,388 non-cardiac surgeries





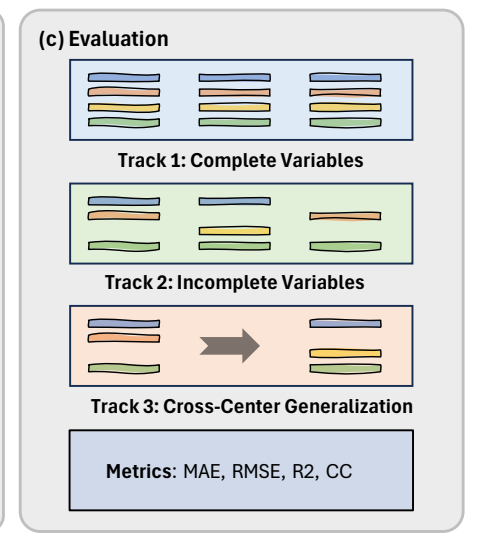


Fig. 1: Overview of the VitalBench Workflow.

performed between August 2016 and June 2017. Each case includes physiological waveforms and structured clinical data sampled at 5-second intervals. We accessed the data via the official API and followed the format of Lee et al. [28] to extract key variables, including demographics, anesthetic parameters, and vital signs, resulting in one wide-format CSV file per surgery, with rows as time steps and columns as variables. After filtering for data quality and completeness while deidentifying patient information, we retained 962 surgeries. See Appendix Table VII for variable details.

MOVER-SIS Dataset. The MOVER dataset, currently the largest open perioperative dataset, includes approximately 59,000 patients' surgical data from around 83,000 surgeries conducted between 2015 and 2022 at the University of California, Irvine Medical Center. The dataset is split into two parts: the SIS (Surgical Information Systems, USA) dataset and the EPIC (Epic Systems, USA) dataset. Given the absence of ventilator parameters in the EPIC dataset, we focused solely on the SIS dataset to align with the variables selected from VitalDB. We extracted a subset from nine long-format tables, reformatted them into wide-format CSV files (one per surgery), and harmonized them with the VitalDB structure. Selected variables include demographics, anesthetic agents, ventilator parameters, and vital signs. After preprocessing and de-identification, 3,221 surgeries were included for analysis. See Appendix Table VIII for full variable list.

C. Data Preprocessing

For each surgical case, we generated input-target pairs by sliding a temporal window across the intraoperative record. Each pair consists of an input sequence $\mathbf{x} \in \mathbb{R}^{L \times K}$ and a target sequence $\mathbf{y} \in \mathbb{R}^{T \times K_d}$, where L denotes the retrospective window length, T the prediction horizon, K the total number of variables, and $K_d \leq K$ the subset of dynamic variables to be forecasted. To handle cold-start conditions, zero-padding was applied to initial steps, but no further preprocessing (e.g., imputation) was used. As shown in Figure 2, VitalDB and

MOVER-SIS exhibit substantial missingness (20-80%) that reflects real clinical dynamics. Imputation could distort these properties; thus, we retained missing values to preserve data fidelity and encourage learning under realistic conditions. The effectiveness of this design is validated in Section IV-C.

D. Masked Loss Function

Since no imputation was performed, we introduced a masked loss function to prevent zero-filled entries from biasing model optimization. Specifically, we applied Mean Squared Error (MSE) as the base objective and applied a binary mask to exclude missing labels from gradient computation:

$$\mathcal{L} = \mathbb{E}_{(\mathbf{x}, \mathbf{y})} \left[\frac{1}{T \cdot K_d} \sum_{t=1}^{T} \sum_{k=1}^{K_d} \mathbf{m}_{t, k} \left(\hat{y}_{t, k} - y_{t, k} \right)^2 \right], \quad (1)$$

where $\mathbf{m} \in 0, 1^{T \times K_d}$ is a binary mask indicating whether each target value is observed $(\mathbf{m}_{t,k} = 1)$ or missing $(\mathbf{m}_{t,k} = 0)$.

This masked formulation ensures that only valid supervision signals contribute to the loss, thereby avoiding distortions introduced by missing entries and maintaining data fidelity.

E. Track Design

To foster clinically reliable forecasting models, VitalBench introduces three progressively challenging tracks that reflect increasing realism in intraoperative data.

Track 1: Complete Variables Data. An idealized track where all physiological variables are fully observed, providing a benchmark for model performance under complete and uninterrupted intraoperative monitoring.

Track 2: Incomplete Variables Data. A realistic clinical setting where some variables are missing due to sensor dropout or incomplete documentation, requiring models to handle sparsity without imputation.

Track 3: Cross-Center Generalization. A transferability test in which models trained at one medical center are evaluated on another, assessing generalization across patient populations, surgical workflows, and monitoring systems.

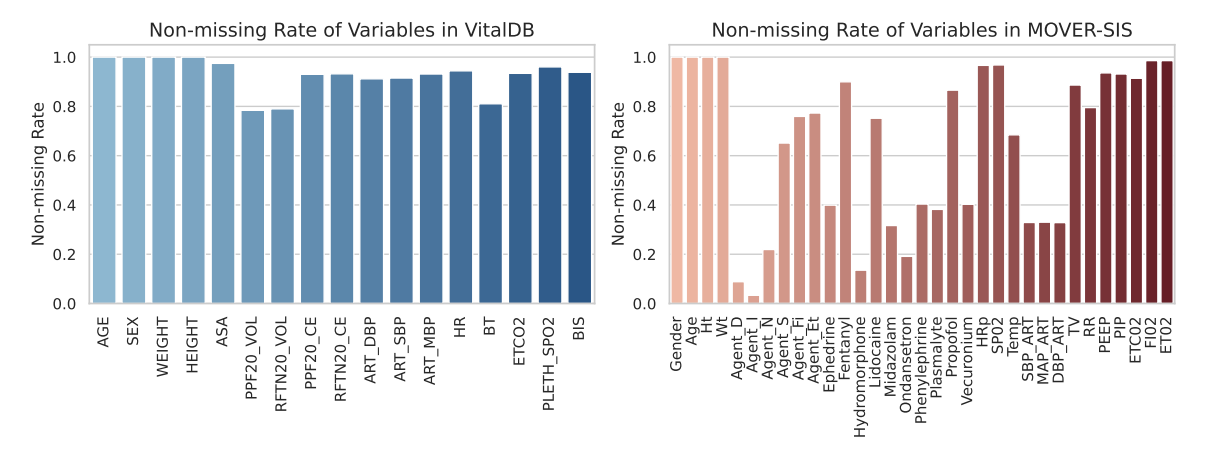


Fig. 2: Non-missing rate of variables across different datasets: VitalDB (left) and MOVER-SIS (right).

TABLE II: Performance comparison of different models on the complete variables track. We report the average performance across different prediction horizons. For the full results, refer to Table IX in the Appendix.

Models Metrics		MambaTS (2024)	LightTS (2023)	iTransformer (2024)	FourierGNN (2024)	PatchTST (2023)	MICN (2024)	DLinear (2023)	S4 (2022)
	MAE	0.034±0.011	0.038±0.011	0.037±0.010	0.040±0.013	0.059±0.064	0.045±0.014	0.055±0.012	0.050 ± 0.013
	RMSE	$0.057 {\pm} 0.015$	0.061 ± 0.015	0.059 ± 0.015	0.064 ± 0.019	0.128 ± 0.067	$0.087 {\pm} 0.025$	0.093 ± 0.018	0.089 ± 0.022
VitalDB	R2	$0.950 {\pm} 0.032$	0.942 ± 0.034	0.947 ± 0.034	$0.937 {\pm} 0.045$	0.594 ± 2.777	$0.863 {\pm} 0.077$	$0.858 {\pm} 0.055$	$0.862 {\pm} 0.065$
	CC	$0.862 {\pm} 0.167$	$0.850 {\pm} 0.168$	$0.862 {\pm} 0.167$	$0.836{\pm}0.190$	$0.787 {\pm} 0.232$	$0.831 {\pm} 0.166$	$0.827{\pm}0.164$	0.821 ± 0.176
SIS	MAE	0.040±0.022	0.044±0.023	0.046±0.034	0.042±0.021	0.058±0.035	0.059 ± 0.070	0.074±0.065	0.067 ± 0.067
₹ -	RMSE	0.080 ± 0.032	$0.081 {\pm} 0.038$	$0.087 {\pm} 0.043$	0.079 ± 0.034	0.127 ± 0.045	$0.137 {\pm} 0.074$	0.130 ± 0.066	$0.133 {\pm} 0.068$
Ĭ.	R2	0.805 ± 1.155	$0.859 {\pm} 0.613$	0.779 ± 1.349	0.807 ± 1.218	0.770 ± 1.024	$0.488{\pm}3.798$	$0.620{\pm}2.353$	0.599 ± 2.634
MOVER-SIS	CC	$0.843 {\pm} 0.173$	0.802 ± 0.203	$0.806 {\pm} 0.222$	$0.823 {\pm} 0.191$	$0.765 {\pm} 0.248$	$0.804{\pm}0.175$	$0.781 {\pm} 0.187$	0.770 ± 0.240

IV. EXPERIMENTS

A. Experimental Setup

Dataset Splitting. The dataset was split based on the chronological order of surgeries, with a 7:1:2 ratio for training, validation, and test sets, ensuring temporal validity.

Baselines and Metrics. We selected a set of state-of-the-art (SOTA) time series forecasting models, representing both variable-independent approaches (e.g., iTransformer [46], LightTS [21], MICN [19], FourierGNN [23], MambaTS [41]) and variable-dependent models (e.g., DLinear [20], PatchTST [40], S4 [49]). Since Tracks 2 and 3 require handling varying input dimensions, models restricted to fixed feature sizes (e.g., LightTS, MICN) were excluded. For all experiments, we used standard evaluation metrics, including Mean Absolute Error (MAE), Root Mean Squared Error (RMSE), R-squared (R²), and Correlation Coefficient (CC), to ensure a comprehensive and consistent assessment of model performance. Lower values for MAE and RMSE indicate better accuracy, while higher values for R² and CC suggest improved model fit and correlation.

Track Design. The VitalDB and MOVER-SIS datasets differ in sampling frequency (12 Hz vs. 1 Hz). Guided by clinical experts, we chose prediction horizons of 1, 3, 10, and 30 minutes, reflecting common clinical needs for intraoperative forecasting. Following Lee et al. [28], a 30-minute retrospec-

tive window was used for both datasets. For VitalDB, this corresponds to 360 input steps and 12, 36, 120, and 360 prediction steps, while for MOVER-SIS, 30 input steps and 1, 3, 10, and 30 prediction steps were used. These configurations were consistently applied across all three tracks, with VitalDB downsampled to 1 Hz in Track 3 to match MOVER-SIS.

In Track 2 and 3, missing data were simulated by randomly dropping variable channels, including static covariates and dynamic physiological variables, while retaining at least one dynamic variable per patient. The same missingness pattern was applied to training, validation, and test to ensure consistent and fair comparisons across baselines.

Implementation Details. Our benchmark was developed primarily using the Time-Series-Library framework [18]. We employed grid search to determine the optimal hyperparameters for each model. For training, we used the Adam optimizer [59] with a total of 10 epochs and a patience of 3 epochs. This configuration was found to be sufficient for model convergence.

B. Benchmark Results

Track 1: Complete Variables Data. Table II reports the average model performance across four prediction horizons, using MAE, RMSE, R^2 , and CC as evaluation metrics. Errors are expressed in the original units of each variable (e.g., beats per minute for heart rate, mmHg for blood pressure, % for

Me	Models	MambaTS (2024)	iTransformer (2024)	FourierGNN (2024)	PatchTST (2023)	Dlinear (2023)	S4 (2022)
~	MAE	0.034±0.004	0.038 ± 0.003	0.039±0.003	0.043±0.005	0.053±0.004	0.049±0.005
VitalDB	RMSE	$0.057 {\pm} 0.003$	0.060 ± 0.004	0.063 ± 0.002	$0.081 {\pm} 0.008$	0.092 ± 0.007	$0.088 {\pm} 0.007$
⁄ita	R2	$0.864{\pm}0.156$	$0.852 {\pm} 0.150$	$0.841 {\pm} 0.154$	0.762 ± 0.177	0.704 ± 0.179	0.734 ± 0.160
	CC	0.839±0.056	$0.829 {\pm} 0.067$	$0.806{\pm}0.055$	0.810 ± 0.045	0.793 ± 0.054	0.794 ± 0.043
SIS	MAE	0.048±0.005	0.052±0.002	0.057±0.006	0.060±0.007	0.073±0.003	0.065±0.006
4	RMSE	$0.097 {\pm} 0.005$	0.102 ± 0.003	0.106 ± 0.006	$0.126 {\pm} 0.005$	0.127 ± 0.003	$0.130 {\pm} 0.005$
ΛĒ	R2	0.835±0.254	$0.820 {\pm} 0.355$	0.829 ± 0.154	0.747 ± 0.303	0.750 ± 0.275	$0.730 {\pm} 0.344$
MOVER-	CC	0.832±0.049	0.812 ± 0.031	$0.808 {\pm} 0.040$	$0.787 {\pm} 0.034$	$0.788 {\pm} 0.047$	0.774 ± 0.038

TABLE III: Performance comparison of different models on the incomplete variables track. We report the average performance across different prediction horizons. For the full results, refer to Table X in the Appendix.

TABLE IV: Performance comparison of different models on the cross-center generalization track. We report the average performance across different prediction horizons. For the full results, refer to Table XI in the Appendix.

Models Metrics		Upper Bound	MambaTS (2024)	iTransformer (2024)	FourierGNN (2024)	PatchTST (2023)	Dlinear (2023)	S4 (2022)				
	$VitalDB \rightarrow MOVER\text{-}SIS$											
	MAE	$0.048 {\pm} 0.005$	0.051 ± 0.005	0.063 ± 0.003	0.070 ± 0.003	0.064 ± 0.009	0.077 ± 0.004	0.067±0.009				
AVG	RMSE	$0.097 {\pm} 0.005$	0.103 ± 0.005	0.116 ± 0.003	0.123 ± 0.004	0.135 ± 0.009	0.129 ± 0.005	0.138 ± 0.010				
A	R2	$0.835 {\pm} 0.254$	0.812 ± 0.212	0.771 ± 0.191	0.745 ± 0.183	0.713 ± 0.321	$0.740{\pm}0.256$	0.705 ± 0.303				
	CC	$0.832{\pm}0.049$	0.816 ± 0.047	0.783 ± 0.041	0.752 ± 0.033	0.777 ± 0.037	0.779 ± 0.035	0.767 ± 0.033				
				$MOVER\text{-}SIS \to$	VitalDB							
	MAE	$0.046{\pm}0.004$	$0.046{\pm}0.004$	0.051 ± 0.004	0.054 ± 0.003	$0.058 {\pm} 0.005$	0.067 ± 0.005	0.063 ± 0.005				
AVG	RMSE	0.075 ± 0.004	0.077 ± 0.005	0.083 ± 0.004	0.086 ± 0.004	0.108 ± 0.007	0.114 ± 0.006	0.112 ± 0.007				
Ā	R2	$0.723 {\pm} 0.581$	0.700 ± 0.457	0.549 ± 0.837	0.573 ± 1.197	$0.354{\pm}0.644$	$0.198{\pm}1.817$	$0.239 {\pm} 0.827$				
	CC	0.809 ± 0.060	0.808 ± 0.062	0.790 ± 0.058	0.772 ± 0.054	0.775 ± 0.048	0.763 ± 0.049	0.763 ± 0.045				

SpO₂), ensuring clinical interpretability. See Tables VII–VIII for more variable definitions and units.

On the VitalDB dataset, MambaTS consistently achieved the best overall performance across all metrics, followed by iTransformer and LightTS. In contrast, model performance on MOVER-SIS showed more variability across tasks and metrics, reflecting higher data heterogeneity. Nonetheless, MambaTS remained a strong performer, with FourierGNN and LightTS also showing competitive results.

Interestingly, variable-independent models (S4, DLinear, PatchTST) consistently underperformed, highlighting the importance of modeling inter-variable dependencies in multivariate vital sign forecasting. Physiological signals are often tightly coupled due to underlying regulatory mechanisms (e.g., cardio-respiratory interactions), and ignoring these relationships can hinder a model's capacity to capture the temporal patient dynamics. Therefore, our findings indicate that models incorporating variable dependencies are better suited for vital sign prediction tasks and tend to achieve superior performance. Track 2: Incomplete Variables Data. This track places more stringent demands on models by requiring them to handle variable numbers of input features across samples. Consequently, fixed-dimension methods (LightTS and MICN) cannot be evaluated in this track. Their exclusion is not intended to bias results, but rather reflects a realistic challenge: intraoperative data often contains missing or intermittently available sensor signals, which these models cannot accommodate.

As a result of increased data incompleteness and heterogeneity, Table III shows a modest performance decline compared to Track 1 (Table II). Despite these challenges, MambaTS consistently outperforms other models, followed by iTransformer and FourierGNN, reflecting their superior capacity to adapt to partial and irregular inputs. Conversely, variable-independent models like S4, DLinear, and PatchTST experience substantial performance drops, highlighting the necessity of modeling inter-variable dependencies to capture physiological couplings under missingness.

Track 3: Cross-Center Generalization. The robustness of vital sign prediction models is essential for ensuring their applicability across diverse clinical settings. As illustrated in Figure 3, principal component analysis (PCA) [60] reveals substantial differences in the distribution of variables between the VitalDB and MOVER-SIS datasets, highlighting the challenges posed by cross-center validation.

To evaluate cross-center generalization, we conducted two transfer experiments: training on VitalDB and testing on MOVER-SIS, and vice versa. For reference, we also report an upper-bound performance, obtained by training MambaTS directly on the target domain, given its strong performance in both Track 1 and Track 2. As shown in Table IV, MambaTS

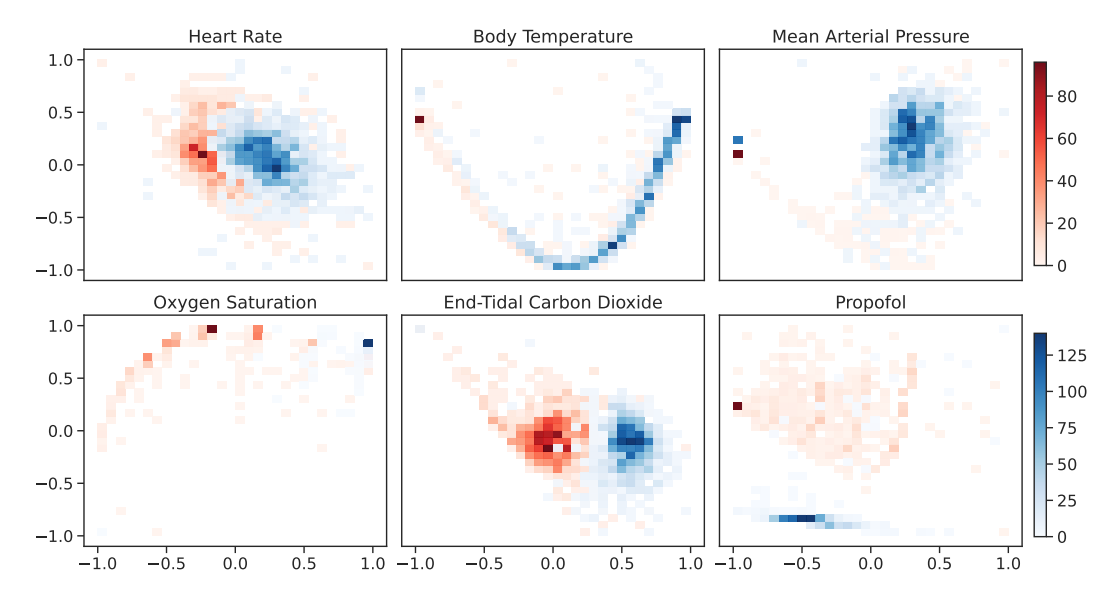


Fig. 3: PCA visualization of representative dynamic variables across datasets. Each subplot shows the first and second principal components for a selected variable, illustrating distributional differences between VitalDB (blue) and MOVER-SIS (red).

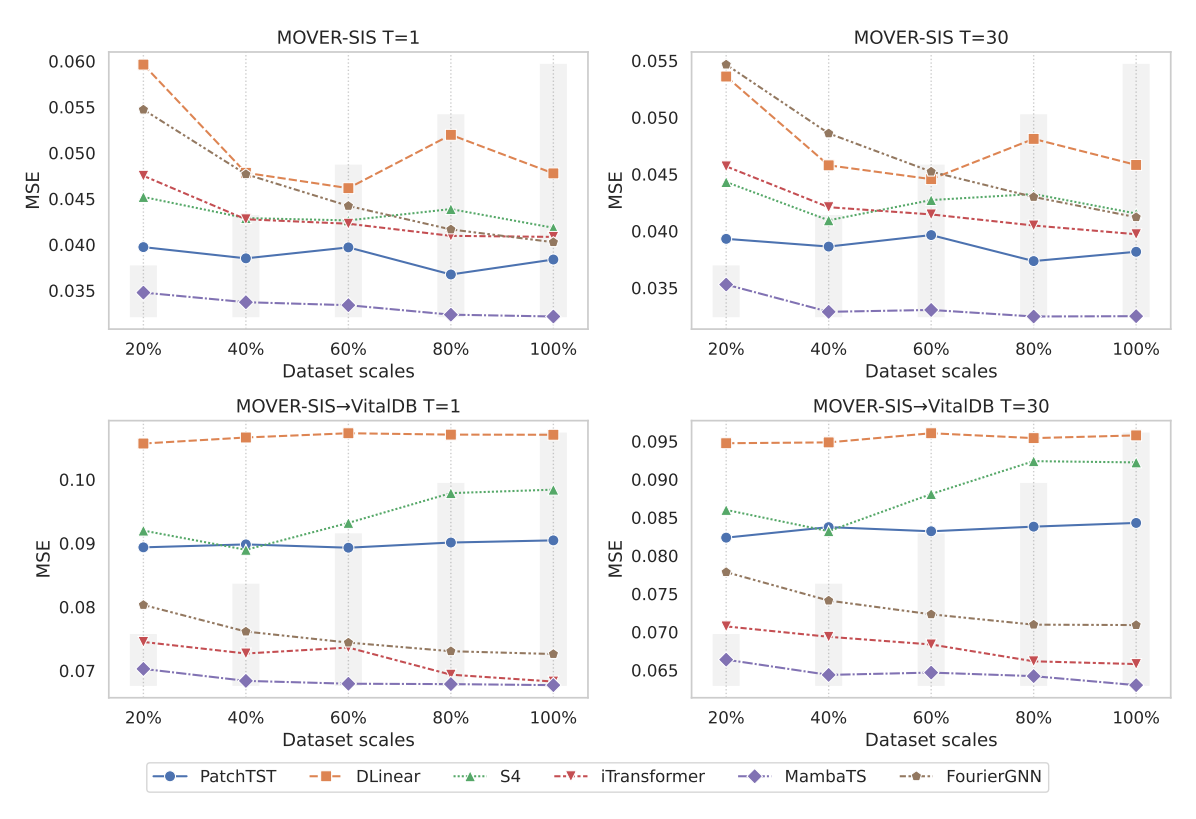


Fig. 4: Performance comparison of different models on datasets of varying scales.

consistently outperformed other baseline models in both directions, with iTransformer performing competitively. Notably, in the MOVER-SIS \rightarrow VitalDB setting, MambaTS achieved performance close to that obtained when trained and tested directly on VitalDB, indicating strong generalization with minimal performance degradation.

In contrast, the VitalDB \rightarrow MOVER-SIS transfer exhibited a larger performance gap, which is likely attributable to the smaller training sample size of VitalDB (962 surgeries)

compared to MOVER-SIS (3,221 surgeries). This discrepancy highlights the critical importance of data scale and diversity in learning generalizable representations. These findings suggest that models trained on sufficiently large and heterogeneous cohorts may effectively transfer to new clinical environments with minimal adaptation. Therefore, expanding training datasets through multi-center collaborations holds strong potential to improve both accuracy and robustness of clinical time-series prediction models in real-world deployments.

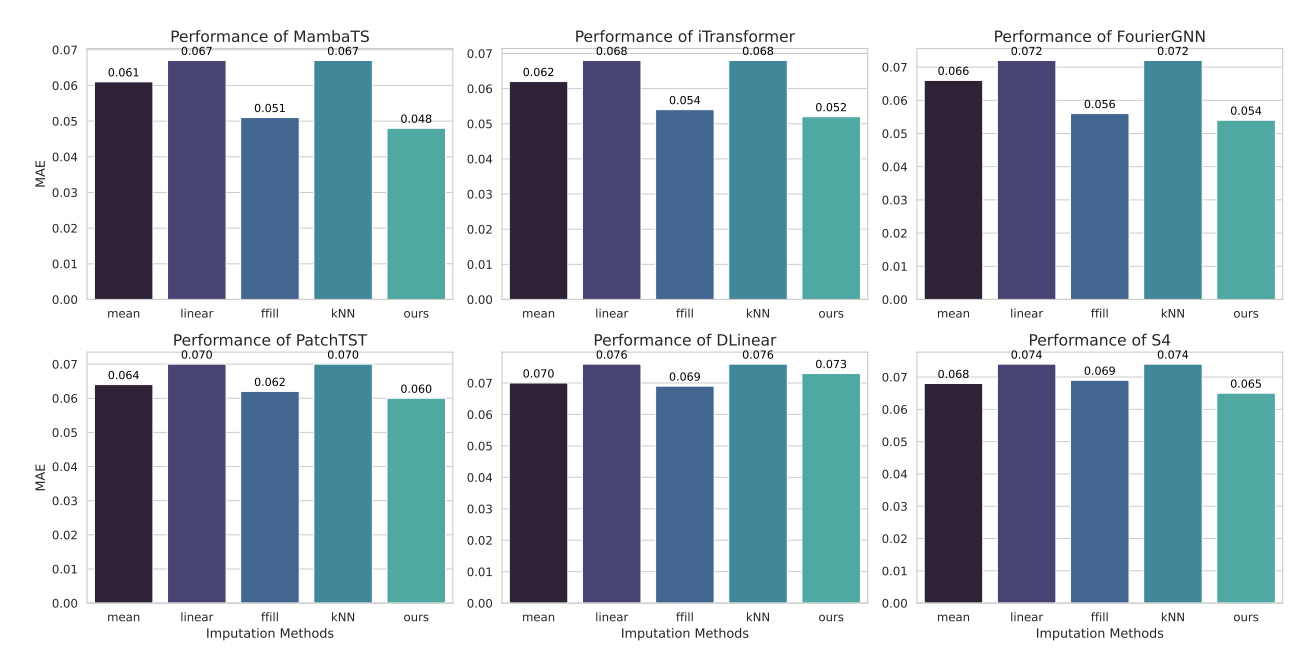


Fig. 5: Comparison of model performance under different data imputation strategies.

C. Ablation Studies

Impact of Data Scale. Extending Track 3 findings, we examined how training size affects model performance (Figure 4). Variable-dependent models (iTransformer, FourierGNN, MambaTS) consistently improve with larger datasets, reflecting their ability to exploit inter-variable relationships essential for robustness across diverse clinical contexts. In contrast, variable-independent models (DLinear, PatchTST, S4) decline as data scale grows, highlighting the limitations of treating each variable independently. These results underscore the critical role of modeling inter-variable dynamics for reliable performance on large, heterogeneous clinical data.

Impact of Imputation. In this section, we analyze the effect of data imputation in VitalBench. As we previously argued, data missingness is an inherent challenge in clinical settings (e.g., prolonged sensor dropouts, as shown in Figure 2). In such cases, imputation can introduce spurious values, distorting predictions of vital signs. To address this, we employ a masked loss function that naturally handles missingness without altering the original data, preserving clinical validity.

Figure 5 compares model performance across four common imputation methods: mean imputation, linear interpolation, forward-fill (ffill), and k-nearest neighbors (kNN). Across nearly all cases, masked loss outperforms these strategies, achieving superior predictive accuracy. DLinear is an exception, showing sensitivity to imputed zeros. While ffill performs reasonably, its reliance on previous values is only valid over short gaps, whereas clinical sensor dropouts often persist longer. These results highlight the importance of explicitly handling missingness rather than relying on imputation for robust and clinically meaningful predictions.

Discussion. Building on our findings, future research in intraoperative vital sign prediction should prioritize models that capture complex inter-variable dependencies, which are

critical for both predictive accuracy and robustness. These models must also accommodate variable input dimensionality to reflect patient heterogeneity and ensure strong cross-center generalization. Equally important is expanding data diversity and scale, as larger multi-center datasets not only enhance performance but also improve generalizability across clinical settings and populations. Integrating these strategies will be essential to develop robust, clinically reliable prediction systems with broad applicability in real-world healthcare.

V. CONCLUSION

In this study, we present VitalBench, a comprehensive benchmark designed to evaluate intraoperative vital sign forecasting models under clinically realistic conditions. By addressing challenges such as incomplete data and cross-center variability, VitalBench provides a rigorous framework for developing robust and generalizable predictive models.

Our experiments yield three key insights. First, accurately modeling inter-variable dependencies is critical. Models such as MambaTS, which capture physiological interactions among vital signs, consistently outperform variable-independent baselines. Second, using a masked loss function that naturally accommodates missing values leads to more reliable predictions than traditional imputation methods, which often introduce artificial noise. Third, increasing the scale and diversity of training data improves generalization performance, but substantial performance gaps remain across clinical centers. This highlights the complexity introduced by variations in patient populations, monitoring protocols, and institutional practices.

VitalBench thus serves as a step toward bridging the gap between algorithmic innovation and clinical deployment. Future efforts should focus on developing models that adapt to varying input dimensions, explicitly handle uncertainty due to missingness, and leverage multi-center datasets to enhance robustness across real-world healthcare environments.

REFERENCES

- [1] N. Kumar, G. Akangire, B. Sullivan, K. Fairchild, and V. Sampath, "Continuous vital sign analysis for predicting and preventing neonatal diseases in the twenty-first century: big data to the forefront," Pediatric research, vol. 87, no. 2, pp. 210–220, 2020.
- [2] C. A. Da Costa, C. F. Pasluosta, B. Eskofier, D. B. Da Silva, and R. da Rosa Righi, "Internet of health things: Toward intelligent vital signs monitoring in hospital wards," <u>Artificial intelligence in medicine</u>, vol. 89, pp. 61–69, 2018.
- [3] N. Kaieski, C. A. Da Costa, R. da Rosa Righi, P. S. Lora, and B. Eskofier, "Application of artificial intelligence methods in vital signs analysis of hospitalized patients: A systematic literature review," <u>Applied Soft</u> Computing, vol. 96, p. 106612, 2020.
- [4] S. Ahmed and S. H. Cho, "Machine learning for healthcare radars: Recent progresses in human vital sign measurement and activity recognition," IEEE Communications Surveys & Tutorials, 2023.
- [5] U. Kyriacos, J. Jelsma, and S. Jordan, "Monitoring vital signs using early warning scoring systems: a review of the literature," <u>Journal of</u> nursing management, vol. 19, no. 3, pp. 311–330, 2011.
- [6] J. Feng, J. Lee, Z. A. Vesoulis, and F. Li, "Predicting mortality risk for preterm infants using deep learning models with time-series vital sign data," npj Digital Medicine, vol. 4, no. 1, p. 108, 2021.
- [7] Æ. Ö. Kristinsson, Y. Gu, S. M. Rasmussen, J. Mølgaard, C. Haahr-Raunkjær, C. S. Meyhoff, E. K. Aasvang, and H. B. Sørensen, "Prediction of serious outcomes based on continuous vital sign monitoring of high-risk patients," <u>Computers in Biology and Medicine</u>, vol. 147, p. 105559, 2022.
- [8] A. Dubatovka, C. B. Nöthiger, D. R. Spahn, J. M. Buhmann, T. R. Roche, and D. W. Tscholl, "Predicting vital sign deviations during surgery from patient monitoring data: developing and validating single-stream deep learning models," <u>British Journal of Anaesthesia</u>, vol. 133, no. 4, pp. 889–892, 2024.
- [9] C. Sun, S. Hong, M. Song, and H. Li, "A review of deep learning methods for irregularly sampled medical time series data," <u>arXiv preprint</u> arXiv:2010.12493, 2020.
- [10] L. Sun, M. Zhang, B. Wang, and P. Tiwari, "Few-shot class-incremental learning for medical time series classification," <u>IEEE Journal of</u> Biomedical and Health Informatics, vol. 28, no. 4, pp. 1872–1882, 2023.
- [11] D. Jarrett, J. Yoon, I. Bica, Z. Qian, A. Ercole, and M. van der Schaar, "Clairvoyance: A pipeline toolkit for medical time series," <u>arXiv:2310.18688</u>, 2023.
- [12] M. Moor, N. Bennett, D. Plečko, M. Horn, B. Rieck, N. Meinshausen, P. Bühlmann, and K. Borgwardt, "Predicting sepsis using deep learning across international sites: a retrospective development and validation study," EClinicalMedicine, vol. 62, 2023.
- [13] D. Zhang, H. Yang, J. Gao, and X. Li, "Imbalanced flight test sensor temporal data anomaly detection," IEEE Transactions on Aerospace and Electronic Systems, vol. 61, no. 2, pp. 2466–2476, 2024.
- [14] D. Salinas, V. Flunkert, J. Gasthaus, and T. Januschowski, "Deepar: Probabilistic forecasting with autoregressive recurrent networks," International Journal of Forecasting, vol. 36, no. 3, pp. 1181–1191, 2020.
- [15] X. Shi, Z. Chen, H. Wang, D. Yeung, W. Wong, and W. Woo, "Convolutional LSTM network: A machine learning approach for precipitation nowcasting," in Advances in Neural Information Processing Systems 28: Annual Conference on Neural Information Processing Systems 2015, December 7-12, 2015, Montreal, Quebec, Canada, C. Cortes, N. D. Lawrence, D. D. Lee, M. Sugiyama, and R. Garnett, Eds., 2015, pp. 802–810.
- [16] G. Lai, W. Chang, Y. Yang, and H. Liu, "Modeling long- and short-term temporal patterns with deep neural networks," in <u>The 41st International ACM SIGIR Conference on Research & Development in Information Retrieval, SIGIR 2018, Ann Arbor, MI, USA, July 08-12, 2018, K. Collins-Thompson, Q. Mei, B. D. Davison, Y. Liu, and E. Yilmaz, Eds. ACM, 2018, pp. 95–104.</u>
- [17] S. Bai, J. Z. Kolter, and V. Koltun, "An empirical evaluation of generic convolutional and recurrent networks for sequence modeling," <u>ArXiv</u> <u>preprint</u>, vol. abs/1803.01271, 2018.
- [18] H. Wu, T. Hu, Y. Liu, H. Zhou, J. Wang, and M. Long, "Timesnet: Temporal 2d-variation modeling for general time series analysis," in <u>The</u> Eleventh International Conference on Learning Representations, ICLR 2023, Kigali, Rwanda, May 1-5, 2023. OpenReview.net, 2023.
- [19] H. Wang, J. Peng, F. Huang, J. Wang, J. Chen, and Y. Xiao, "MICN: multi-scale local and global context modeling for long-term series forecasting," in The Eleventh International Conference on Learning Representations, ICLR 2023, Kigali, Rwanda, May 1-5, 2023. Open-Review.net, 2023.

- [20] A. Zeng, M. Chen, L. Zhang, and Q. Xu, "Are transformers effective for time series forecasting?" in Thirty-Seventh AAAI Conference on Artificial Intelligence, AAAI 2023, Thirty-Fifth Conference on Innovative Applications of Artificial Intelligence, IAAI 2023, Thirteenth Symposium on Educational Advances in Artificial Intelligence, EAAI 2023, Washington, DC, USA, February 7-14, 2023, B. Williams, Y. Chen, and J. Neville, Eds. AAAI Press, 2023, pp. 11 121-11 128.
- [21] T. Zhang, Y. Zhang, W. Cao, J. Bian, X. Yi, S. Zheng, and J. Li, "Less is more: Fast multivariate time series forecasting with light samplingoriented mlp structures," arXiv preprint arXiv:2207.01186, 2022.
- [22] Z. Wu, S. Pan, G. Long, J. Jiang, X. Chang, and C. Zhang, "Connecting the dots: Multivariate time series forecasting with graph neural networks," in KDD '20: The 26th ACM SIGKDD Conference on Knowledge Discovery and Data Mining, Virtual Event, CA, USA, August 23-27, 2020, R. Gupta, Y. Liu, J. Tang, and B. A. Prakash, Eds. ACM, 2020, pp. 753-763.
- [23] K. Yi, Q. Zhang, W. Fan, H. He, L. Hu, P. Wang, N. An, L. Cao, and Z. Niu, "Fouriergnn: Rethinking multivariate time series forecasting from a pure graph perspective," in <u>Advances in Neural Information Processing Systems</u> 36: Annual Conference on Neural Information Processing Systems 2023, NeurIPS 2023, New Orleans, LA, USA, December 10 16, 2023, A. Oh, T. Naumann, A. Globerson, K. Saenko, M. Hardt, and S. Levine, Eds., 2023.
- [24] H. Zhou, S. Zhang, J. Peng, S. Zhang, J. Li, H. Xiong, and W. Zhang, "Informer: Beyond efficient transformer for long sequence time-series forecasting," in Thirty-Fifth AAAI Conference on Artificial Intelligence, AAAI 2021, Thirty-Third Conference on Innovative Applications of Artificial Intelligence, IAAI 2021, The Eleventh Symposium on Educational Advances in Artificial Intelligence, EAAI 2021, Virtual Event, February 2-9, 2021. AAAI Press, 2021, pp. 11 106–11 115.
- [25] T. Zhou, Z. Ma, Q. Wen, X. Wang, L. Sun, and R. Jin, "Fedformer: Frequency enhanced decomposed transformer for long-term series forecasting," in <u>International Conference on Machine Learning, ICML 2022</u>, 17-23 <u>July 2022</u>, Baltimore, Maryland, USA, ser. Proceedings of Machine Learning Research, K. Chaudhuri, S. Jegelka, L. Song, C. Szepesvári, G. Niu, and S. Sabato, Eds., vol. 162. PMLR, 2022, pp. 27 268–27 286.
- [26] Z. Li, W. Guo, J. An, Q. Wang, Y. Mei, R. Juan, T. Wang, Y. Li, and Z. Gao, "Ad2t: Multivariate time-series anomaly detection with association discrepancy dual-decoder transformer," <u>IEEE Sensors Journal</u>, vol. 25, no. 7, pp. 11710–11721, 2025.
- [27] Y.-L. He, Z.-H. Bai, Y. Xu, Q.-X. Zhu, and L. Li, "Patch-decompositionenhanced tcn with transformer for soft sensor modeling," <u>IEEE Sensors</u> Journal, pp. 1–1, 2025.
- [28] S. Lee, H.-C. Lee, Y. S. Chu, S. W. Song, G. J. Ahn, H. Lee, S. Yang, and S. B. Koh, "Deep learning models for the prediction of intraoperative hypotension," <u>British journal of anaesthesia</u>, vol. 126, no. 4, pp. 808– 817, 2021.
- [29] Y.-F. Chen, S.-Z. Fan, M. F. Abbod, J.-S. Shieh, and M. Zhang, "Nonlinear analysis of electroencephalogram variability as a measure of the depth of anesthesia," <u>IEEE Transactions on Instrumentation and Measurement</u>, vol. 71, pp. 1–13, 2022.
- [30] N. Bahador, J. Jokelainen, S. Mustola, and J. Kortelainen, "Multimodal spatio-temporal-spectral fusion for deep learning applications in physiological time series processing: A case study in monitoring the depth of anesthesia," <u>Information Fusion</u>, vol. 73, pp. 125–143, 2021.
- [31] Y. He, S. Peng, M. Chen, Z. Yang, and Y. Chen, "A transformer-based prediction method for depth of anesthesia during target-controlled infusion of propofol and remifentanil," <u>IEEE Transactions on Neural Systems and Rehabilitation Engineering</u>, 2023.
- [32] H. Yèche, R. Kuznetsova, M. Zimmermann, M. Hüser, X. Lyu, M. Faltys, and G. Rätsch, "Hirid-icu-benchmark—a comprehensive machine learning benchmark on high-resolution icu data," <u>arXiv preprint</u> arXiv:2111.08536, 2021.
- [33] P. Rockenschaub, A. Hilbert, T. Kossen, P. Elbers, F. von Dincklage, V. I. Madai, and D. Frey, "The impact of multi-institution datasets on the generalizability of machine learning prediction models in the icu," Critical Care Medicine, vol. 52, no. 11, pp. 1710–1721, 2024.
- [34] H.-C. Lee, Y. Park, S. B. Yoon, S. M. Yang, D. Park, and C.-W. Jung, "Vitaldb, a high-fidelity multi-parameter vital signs database in surgical patients," Scientific Data, vol. 9, no. 1, p. 279, 2022.
- [35] M. Samad, M. Angel, J. Rinehart, Y. Kanomata, P. Baldi, and M. Cannesson, "Medical informatics operating room vitals and events repository (mover): a public-access operating room database," <u>JAMIA open</u>, vol. 6, no. 4, p. ooad084, 2023.
- [36] A. Trindade, "ElectricityLoadDiagrams20112014," UCI Machine Learning Repository, 2015, DOI: https://doi.org/10.24432/C58C86.

- [37] H. Wu, J. Xu, J. Wang, and M. Long, "Autoformer: Decomposition transformers with auto-correlation for long-term series forecasting," in Advances in Neural Information Processing Systems 34: Annual Conference on Neural Information Processing Systems 2021, NeurIPS 2021, December 6-14, 2021, virtual, M. Ranzato, A. Beygelzimer, Y. N. Dauphin, P. Liang, and J. W. Vaughan, Eds., 2021, pp. 22419–22430.
- [38] G. Panagopoulos, G. Nikolentzos, and M. Vazirgiannis, "Transfer graph neural networks for pandemic forecasting," in <u>Thirty-Fifth AAAI Conference on Artificial Intelligence</u>, AAAI 2021, <u>Thirty-Third Conference on Innovative Applications of Artificial Intelligence</u>, IAAI 2021, The Eleventh Symposium on Educational Advances in Artificial Intelligence, EAAI 2021, Virtual Event, February 2-9, 2021. AAAI Press, 2021, pp. 4838–4845.
- [39] G. E. Box and D. A. Pierce, "Distribution of residual autocorrelations in autoregressive-integrated moving average time series models," <u>Journal</u> of the <u>American statistical Association</u>, vol. 65, no. 332, pp. 1509–1526, 1970
- [40] Y. Nie, N. H. Nguyen, P. Sinthong, and J. Kalagnanam, "A time series is worth 64 words: Long-term forecasting with transformers," in The Eleventh International Conference on Learning Representations, ICLR 2023, Kigali, Rwanda, May 1-5, 2023. OpenReview.net, 2023.
 [41] X. Cai, Y. Zhu, X. Wang, and Y. Yao, "Mambats: Improved selective
- [41] X. Cai, Y. Zhu, X. Wang, and Y. Yao, "Mambats: Improved selective state space models for long-term time series forecasting," <u>arXiv preprint</u> arXiv:2405.16440, 2024.
- [42] A. Patharkar, F. Al-Hindawi, and T. Wu, "Healthy bio-core: A framework for selection of homogeneous healthy biomedical multivariate time series employing classification performance," <u>IEEE Journal of Biomedical and Health Informatics</u>, pp. 1–14, 2025.
- [43] D. Zhang, J. Gao, and X. Li, "Learning long-range relationships for temporal aircraft anomaly detection," IEEE Transactions on Aerospace and Electronic Systems, vol. 60, no. 5, pp. 6385–6395, 2024.
- [44] A. Vaswani, N. Shazeer, N. Parmar, J. Uszkoreit, L. Jones, A. N. Gomez, L. Kaiser, and I. Polosukhin, "Attention is all you need," in <u>Advances in Neural Information Processing Systems 30: Annual Conference on Neural Information Processing Systems 2017, December 4-9, 2017, Long Beach, CA, USA, I. Guyon, U. von Luxburg, S. Bengio, H. M. Wallach, R. Fergus, S. V. N. Vishwanathan, and R. Garnett, Eds., 2017, pp. 5998–6008.</u>
- [45] M. Jiang, Y. Li, J. He, Y. Yang, H. Xie, and X. Chen, "Physiological time-series fusion with hybrid attention for adaptive recognition of pain," <u>IEEE Journal of Biomedical and Health Informatics</u>, vol. 28, no. 11, pp. 6865–6873, 2024.
- [46] Y. Liu, T. Hu, H. Zhang, H. Wu, S. Wang, L. Ma, and M. Long, "itransformer: Inverted transformers are effective for time series forecasting," in <u>International Conference on Learning Representations (ICLR)</u>, 2024.
- [47] Z. Xu, J. Guo, L. Qin, Y. Xie, Y. Xiao, X. Lin, Q. Li, and X. Li, "Predicting icu interventions: A transparent decision support model based on multivariate time series graph convolutional neural network," IEEE Journal of Biomedical and Health Informatics, vol. 28, no. 6, pp. 3709–3720, 2024.

- [48] D. Y. Fu, T. Dao, K. K. Saab, A. W. Thomas, A. Rudra, and C. Ré, "Hungry hungry hippos: Towards language modeling with state space models," in The Eleventh International Conference on Learning Representations, ICLR 2023, Kigali, Rwanda, May 1-5, 2023. Open-Review.net, 2023.
- [49] A. Gu, K. Goel, and C. Ré, "Efficiently modeling long sequences with structured state spaces," in <u>The Tenth International Conference on Learning Representations, ICLR 2022</u>, Virtual Event, April 25-29, 2022. OpenReview.net, 2022.
- [50] M. Zhang, K. K. Saab, M. Poli, T. Dao, K. Goel, and C. Ré, "Effectively modeling time series with simple discrete state spaces," in <u>The Eleventh International Conference on Learning Representations</u>, <u>ICLR 2023</u>, <u>Kigali</u>, Rwanda, May 1-5, 2023. OpenReview.net, 2023.
- [51] A. Gu and T. Dao, "Mamba: Linear-time sequence modeling with selective state spaces," <u>ArXiv preprint</u>, vol. abs/2312.00752, 2023.
- [52] A. Saporta, X. Gui, A. Agrawal, A. Pareek, S. Q. Truong, C. D. Nguyen, V.-D. Ngo, J. Seekins, F. G. Blankenberg, A. Y. Ng et al., "Benchmarking saliency methods for chest x-ray interpretation," Nature Machine Intelligence, vol. 4, no. 10, pp. 867–878, 2022.
- [53] Y. Ektefaie, A. Shen, D. Bykova, M. G. Marin, M. Zitnik, and M. Farhat, "Evaluating generalizability of artificial intelligence models for molecular datasets," <u>Nature Machine Intelligence</u>, pp. 1–13, 2024.
- [54] A. Bauer, M. Züfle, S. Eismann, J. Grohmann, N. Herbst, and S. Kounev, "Libra: A benchmark for time series forecasting methods," in <u>Proceedings of the ACM/SPEC International Conference on Performance Engineering</u>, 2021, pp. 189–200.
- [55] X. Qiu, J. Hu, L. Zhou, X. Wu, J. Du, B. Zhang, C. Guo, A. Zhou, C. S. Jensen, Z. Sheng et al., "Tfb: Towards comprehensive and fair benchmarking of time series forecasting methods," <u>ArXiv preprint</u>, vol. abs/2403.20150, 2024.
- [56] H. Harutyunyan, H. Khachatrian, D. C. Kale, G. Ver Steeg, and A. Galstyan, "Multitask learning and benchmarking with clinical time series data," Scientific data, vol. 6, no. 1, p. 96, 2019.
- [57] A. E. Johnson, T. J. Pollard, L. Shen, L.-w. H. Lehman, M. Feng, M. Ghassemi, B. Moody, P. Szolovits, L. Anthony Celi, and R. G. Mark, "Mimic-iii, a freely accessible critical care database," <u>Scientific data</u>, vol. 3, no. 1, pp. 1–9, 2016.
- [58] R. V. D. Water, H. Schmidt, P. W. G. Elbers, P. Thoral, B. Arnrich, and P. Rockenschaub, "Yet another ICU benchmark: A flexible multi-center framework for clinical ML," in <u>The Twelfth International Conference</u> on Learning Representations, ICLR 2024, Vienna, Austria, May 7-11, 2024. OpenReview.net. 2024.
- [59] D. P. Kingma and J. Ba, "Adam: A method for stochastic optimization," in 3rd International Conference on Learning Representations, ICLR 2015, San Diego, CA, USA, May 7-9, 2015, Conference Track Proceedings, Y. Bengio and Y. LeCun, Eds., 2015.
- [60] S. Wold, K. Esbensen, and P. Geladi, "Principal component analysis," <u>Chemometrics and intelligent laboratory systems</u>, vol. 2, no. 1-3, pp. 37–52, 1987.

Supplementary Materials for VitalBench: A Rigorous Multi-Center Benchmark for Long-Term Vital Sign Prediction in Intraoperative Care

VITALDB DATASET

The **VitaIDB dataset** [34] is a publicly available, single-center perioperative dataset that includes detailed anesthesia records from 6,388 non-cardiac surgeries performed between August 2016 and June 2017 at Seoul National University Hospital, South Korea. The dataset provides comprehensive perioperative monitoring data, including physiological signals, anesthetic parameters, and demographic information. VitaIDB is accessible at https://vitaldb.net/, offering open access to synchronized intraoperative waveforms, trends, and event data for research and educational purposes.

Inclusion and Exclusion Criteria

The following criteria were applied for patient inclusion:

- Surgery duration of at least 2 hours
- General anesthesia administered throughout the procedure
- Age of 18 years or older
- Weight greater than 35 kg

After applying these criteria, 962 surgeries were included for analysis. The statistical information regarding the dataset division is presented in Table V.

Variables in the Dataset

As shown in Table VII, each surgery record in the VitalDB dataset includes 17 variables, divided into the following categories:

- **Demographic Data**: 'Age', 'Gender', 'Weight', 'Height', 'ASA'
- Anesthetic Information: 'Orchestra/PPF20_VOL', 'Orchestra/RFTN20_VOL', 'Orchestra/PPF20_CE', 'Orchestra/

RFTN20_CE'

Vital Signs: 'Solar8000/ART_DBP', 'Solar8000/ART_SBP', 'Solar8000/ART_MBP', 'Solar8000/HR', 'Solar8000/BT', 'Solar8000/ETCO2', 'Solar8000/PLETH_SPO2', 'BIS/BIS'

Among these, demographic variables serve as constant features and act as covariates for modeling other dynamic variables, with operation type also reported for reference. The overall demographic and surgical characteristics of the VitalDB cohort are summarized in Figure 6.

MOVER-SIS DATASET

The MOVER-SIS dataset, a subset of the largest publicly available perioperative dataset [35], includes data from 19,114 patients who underwent surgeries at the University of California, Irvine Medical Center between 2015 and 2017. It contains rich perioperative information, such as demographic details, medication records, ventilator parameters, and vital signs collected through the Surgical Information System (SIS). The dataset is available at https://mover.ics.uci.edu/and was used under the UCI-OR Data Use Agreement.

Inclusion and Exclusion Criteria

The inclusion and exclusion criteria for the MOVER-SIS dataset are identical to those used in the VitalDB dataset:

- Surgery duration of at least 2 hours
- General anesthesia administered throughout the procedure
- · Age of 18 years or older
- Weight greater than 35 kg

The final dataset contains records from all eligible surgeries meeting these criteria. The statistical information regarding the dataset division is presented in Table VI.

Variables in the Dataset

As shown in VIII, each surgery record in the MOVER-SIS dataset includes 33 variables, categorized as follows:

- Demographic Data: 'Age', 'Gender', 'Height', 'Weight'
- Anesthetic Information: 'Agent_D', 'Agent_I', 'Agent_N', 'Agent_S', 'Agent_Fi', 'Agent_Et', 'Ephedrine', 'Fentanyl', 'Hydromorphone', 'Lidocaine', 'Midazolam', 'Ondansetron', 'Phenylephrine', 'Plasmalyte', 'Propofol', 'Vecuronium'
- Vital Signs: 'HRp', 'SP02', 'Temp', 'SBP_ART', 'MAP_ART', 'DBP_ART'
- Ventilator Parameters: 'TV', 'RR', 'PEEP', 'PIP', 'ETCO2', 'FI02', 'ET02'

Similar to the VitalDB cohort, demographic variables in the MOVER-SIS dataset remain constant throughout each surgery and serve as covariates for predicting other physiological and pharmacological signals, with operation type also reported for reference. Figure 7 summarizes the demographic distributions and surgical characteristics of the MOVER-SIS cohort.

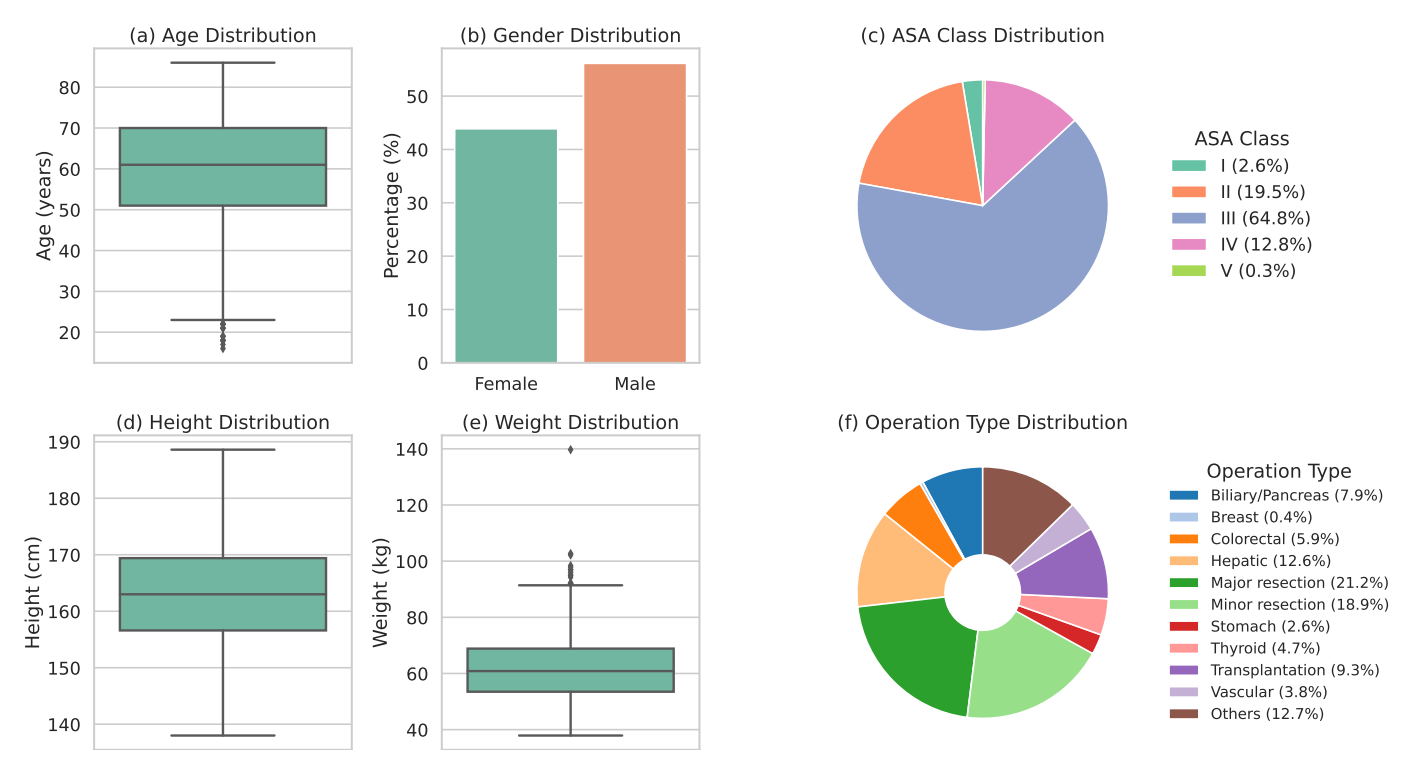


Fig. 6: Summary of patient demographics and surgical characteristics in the VitalDB cohort. Box plots illustrate the distributions of age (a), height (d) and weight (e), while bar plots summarize the gender (b) distributions. The pie charts display the proportions of ASA classes (c) and operation types (f).

TABLE V: Summary of Demographic and Clinical Variables across Different Cohorts in VitalDB.

Variable	Overall	Training	Validation	Test	P-Value	P-Test
n	962	673	96	193		
Age, median [Q1, Q3]	61.0 [51.0, 70.0]	61.0 [52.0, 70.0]	60.5 [53.8, 70.0]	60.0 [51.0, 70.0]	0.962	Kruskal-Wallis
Gender, n (%)						
Female	422 (43.9)	296 (44.0)	48 (50.0)	78 (40.4)	0.301	Chi-squared
Male	540 (56.1)	377 (56.0)	48 (50.0)	115 (59.6)		1
Height, median [Q1, Q3]	163.0 [156.6, 169.4]	163.0 [156.5, 169.3]	161.2 [154.4, 169.9]	164.1 [157.3, 170.0]	0.175	Kruskal-Wallis
Weight, median [Q1, Q3]	60.8 [53.5, 68.9]	60.8 [53.8, 68.2]	58.6 [51.1, 70.3]	62.2 [54.0, 71.2]	0.272	Kruskal-Wallis
ASA, n (%)						
I	25 (2.6)	15 (2.2)	2 (2.1)	8 (4.1)	0.412	Chi-squared
II	188 (19.5)	131 (19.5)	21 (21.9)	36 (18.7)		•
III	623 (64.8)	445 (66.1)	55 (57.3)	123 (63.7)		
IV	123 (12.8)	81 (12.0)	17 (17.7)	25 (13.0)		
V	3 (0.3)	1 (0.1)	1 (1.0)	1 (0.5)		
Operation Type, n (%)						
Biliary/Pancreas	76 (7.9)	46 (6.8)	11 (11.5)	19 (9.8)	0.554	Chi-squared
Breast	4 (0.4)	3 (0.4)	1 (1.0)			•
Colorectal	57 (5.9)	39 (5.8)	7 (7.3)	11 (5.7)		
Hepatic	121 (12.6)	80 (11.9)	14 (14.6)	27 (14.0)		
Major resection	204 (21.2)	140 (20.8)	25 (26.0)	39 (20.2)		
Minor resection	182 (18.9)	138 (20.5)	12 (12.5)	32 (16.6)		
Stomach	25 (2.6)	16 (2.4)	4 (4.2)	5 (2.6)		
Thyroid	45 (4.7)	30 (4.5)	5 (5.2)	10 (5.2)		
Transplantation	89 (9.3)	61 (9.1)	6 (6.2)	22 (11.4)		
Vascular	37 (3.8)	25 (3.7)	4 (4.2)	8 (4.1)		
Others	122 (12.7)	95 (14.1)	7 (7.3)	20 (10.4)		

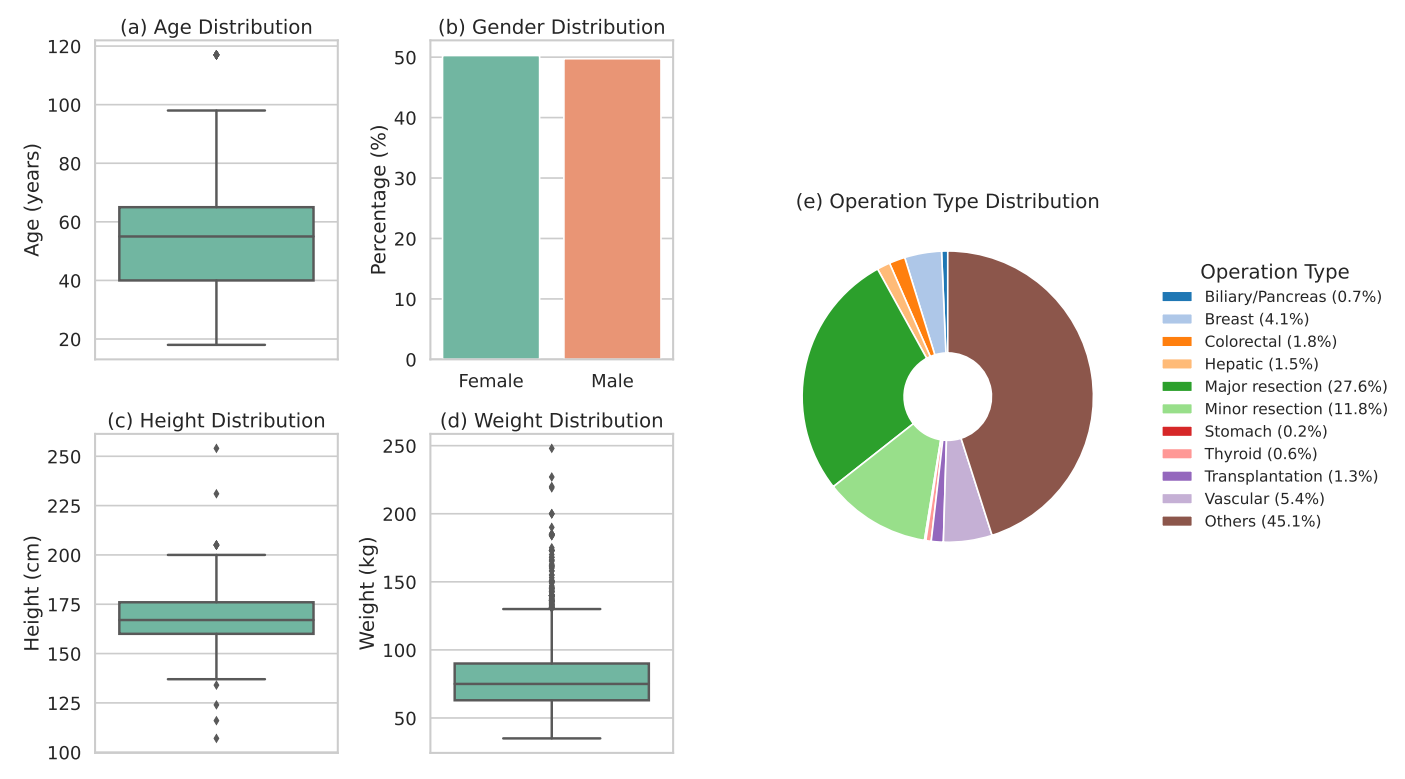


Fig. 7: Summary of patient demographics and surgical characteristics in the MOVER-SIS cohort. Box plots illustrate the distributions of age (a), height (c) and weight (d), while bar plots summarize the gender (b) distributions. The pie chart presents the proportions of different operation types (e).

TABLE VI: Summary of Demographic and Clinical Variables across Different Cohorts in MOVER-SIS.

Variable	Overall	Training	Validation	Test	P-Value	P-Test
n	3221	2254	322	645		
Age, median [Q1, Q3]	55.0 [40.0, 65.0]	54.0 [40.0, 65.0]	57.0 [44.0, 66.0]	55.0 [42.0, 66.0]	0.235	Kruskal-Wallis
Gender, n (%)	1610 (50.2)	1120 (50.1)	150 (40.4)	220 (51.2)	0.050	CI : 1
Female	1619 (50.3)	1130 (50.1)	159 (49.4)	330 (51.2)	0.850	Chi-squared
Male	1602 (49.7)	1124 (49.9)	163 (50.6)	315 (48.8)		
Height, median [Q1, Q3]	167.0 [160.0, 176.0]	167.0 [160.0, 175.0]	167.0 [160.0, 177.0]	167.0 [160.0, 177.0]	0.567	Kruskal-Wallis
Weight, median [Q1, Q3]	75.0 [63.0, 90.0]	75.0 [63.0, 90.0]	76.5 [61.0, 92.8]	75.0 [65.0, 88.0]	0.854	Kruskal-Wallis
Operation Type, n (%)						
Biliary/Pancreas	22 (0.7)	13 (0.6)	4 (1.2)	5 (0.8)	0.965	Chi-squared
Breast	132 (4.1)	93 (4.1)	13 (4.0)	26 (4.0)		•
Colorectal	57 (1.8)	42 (1.9)	3 (0.9)	12 (1.9)		
Hepatic	47 (1.5)	38 (1.7)	5 (1.6)	4 (0.6)		
Major resection	889 (27.6)	622 (27.6)	90 (28.0)	177 (27.4)		
Minor resection	381 (11.8)	262 (11.6)	41 (12.7)	78 (12.1)		
Stomach	5 (0.2)	4 (0.2)	· · · · · · · · · · · · · · · · · · ·	1 (0.2)		
Thyroid	19 (0.6)	13 (0.6)	3 (0.9)	3 (0.5)		
Transplantation	43 (1.3)	28 (1.2)	5 (1.6)	10 (1.6)		
Vascular	174 (5.4)	118 (5.2)	18 (5.6)	38 (5.9)		
Others	1452 (45.1)	1021 (45.3)	140 (43.5)	291 (45.1)		

TABLE VII: Summary of Variables Selected from the VitalDB Dataset.

Variable	Description	Unit	Covariate
Age	Age of the patient	years	<u>√</u>
Gender	Gender of the patient	_	\checkmark
Weight	Body weight of the patient	kg	\checkmark
Height	Height of the patient	cm	\checkmark
ASA	ASA classification	_	\checkmark
Orchestra/PPF20_VOL	Propofol infusion volume	mL	
Orchestra/RFTN20_VOL	Remifentanil infusion volume	mL	
Orchestra/PPF20_CE	Propofol effect-site concentration	μ g/mL	
Orchestra/RFTN20_CE	Remifentanil effect-site concentration	ng/mL	
Solar8000/HR	Heart rate	bpm	
Solar8000/BT	Body temperature	°Ĉ	
Solar8000/ART_DBP	Arterial diastolic blood pressure	mmHg	
Solar8000/ART_SBP	Arterial systolic blood pressure	mmHg	
Solar8000/ART_MBP	Arterial mean blood pressure	mmHg	
Solar8000/ETCO2	End-tidal carbon dioxide	mmHg	
Solar8000/PLETH_SPO2	Peripheral oxygen saturation	%	
BIS/BIS	Bispectral index	[0-100]	

TABLE VIII: Summary of Variables Selected from the MOVER-SIS Dataset.

Variable	Description	Unit	Covariate
Age	Age of the patient	years	√
Gender	Gender of the patient	_	\checkmark
Wt	Body weight of the patient	kg	√
Ht	Height of the patient	cm	\checkmark
ASA	ASA classification	_	\checkmark
Agent_D	Dose of agent D	mL	
Agent_I	Dose of agent I	mL	
Agent_N	Dose of agent N	mL	
Agent_S	Dose of agent S	mL	
Agent_Fi	Inspired concentration of agent	%	
Agent_Et	End-tidal concentration of agent	%	
Ephedrine	Ephedrine dose	mg	
Fentanyl	Fentanyl dose	μg	
Hydromorphone	Hydromorphone dose	mg	
Lidocaine	Lidocaine dose	mg	
Midazolam	Midazolam dose	mg	
Ondansetron	Ondansetron dose	mg	
Phenylephrine	Phenylephrine dose	μg	
Plasmalyte	Plasmalyte dose	mL	
Propofol	Propofol dose	mg	
Vecuronium	Vecuronium dose	mg	
HRp	Heart rate (postoperative)	bpm	
SpO2	Peripheral oxygen saturation	%	
Temp	Body temperature	°C	
SBP_ART	Systolic blood pressure	mmHg	
MAP_ART	Mean arterial pressure	mmHg	
DBP_ART	Diastolic blood pressure	mmHg	
TV	Tidal volume	mL	
RR	Respiratory rate	breaths/min	
PEEP	Positive end-expiratory pressure	cmH ₂ O	
PIP	Peak inspiratory pressure	cmH ₂ O	
ETCO2	End-tidal CO ₂	mmĤg	
FI02	Inspired oxygen concentration	%	
ET02	End-tidal oxygen concentration	%	

TABLE IX: Full performance comparison of different models on the complete variables track. The historical window is set to 30 minutes, and the forecasting horizons are 1, 3, 10, and 30 minutes.

Met	Models	MambaTS (2024)	LightTS (2023)	iTransformer (2024)	FourierGNN (2024)	PatchTST (2023)	MICN (2024)	DLinear (2023)	S4 (2022)
					VitalDB				
	MAE	0.022±0.007	0.026±0.007	0.027±0.006	0.031±0.009	0.038±0.073	0.031±0.009	0.028±0.007	0.034 ± 0.008
	RMSE	$0.041 {\pm} 0.009$	0.046 ± 0.010	0.045 ± 0.010	0.052 ± 0.014	0.090 ± 0.072	0.062 ± 0.016	0.061 ± 0.013	0.063 ± 0.012
1	R2	0.977 ± 0.013	0.971 ± 0.014	0.973 ± 0.013	0.962 ± 0.022	0.844 ± 0.892	0.942 ± 0.028	0.946 ± 0.024	0.941 ± 0.024
	CC	$0.930 {\pm} 0.083$	0.918 ± 0.085	0.927 ± 0.084	0.895 ± 0.115	0.866 ± 0.192	0.905 ± 0.084	0.914 ± 0.088	0.899 ± 0.092
	MAE	$0.028 {\pm} 0.010$	0.034 ± 0.010	0.034 ± 0.008	0.035 ± 0.012	0.044 ± 0.072	0.036 ± 0.011	0.040 ± 0.010	0.040 ± 0.010
2	RMSE	$0.051 {\pm} 0.012$	0.056 ± 0.013	0.053 ± 0.013	$0.058 {\pm} 0.018$	0.108 ± 0.071	0.073 ± 0.018	0.077 ± 0.015	0.075 ± 0.015
3	R2	$0.965 {\pm} 0.019$	0.955 ± 0.022	0.961 ± 0.020	0.952 ± 0.032	0.755 ± 1.551	0.919 ± 0.038	0.914 ± 0.034	0.916 ± 0.037
	CC	$0.899 {\pm} 0.123$	$0.883 {\pm} 0.126$	$0.896 {\pm} 0.126$	0.870 ± 0.149	$0.835{\pm}0.218$	$0.874 {\pm} 0.126$	$0.875 {\pm} 0.131$	0.863 ± 0.134
	MAE	$0.035 {\pm} 0.012$	0.042±0.013	0.040 ± 0.012	0.044 ± 0.015	0.064 ± 0.054	0.048 ± 0.015	0.061 ± 0.013	0.054 ± 0.013
10	RMSE	0.061 ± 0.017	$0.068 {\pm} 0.018$	0.065 ± 0.018	0.070 ± 0.023	0.138 ± 0.059	0.092 ± 0.025	0.102 ± 0.019	0.097 ± 0.022
10	R2	$0.947{\pm}0.036$	0.931 ± 0.040	0.940 ± 0.038	$0.926{\pm}0.058$	0.570 ± 3.051	$0.864 {\pm} 0.069$	$0.844 {\pm} 0.060$	0.851 ± 0.069
	CC	$0.850 {\pm} 0.185$	$0.832{\pm}0.188$	$0.847 {\pm} 0.188$	0.819 ± 0.211	0.763 ± 0.249	0.807 ± 0.192	$0.801 {\pm} 0.189$	0.797 ± 0.207
	MAE	0.051 ± 0.013	0.048 ± 0.015	$0.046 {\pm} 0.015$	0.049 ± 0.016	0.092 ± 0.055	0.066 ± 0.023	0.090 ± 0.019	0.071 ± 0.022
30	RMSE	0.076 ± 0.021	0.074 ± 0.021	0.074 ± 0.021	0.076 ± 0.023	0.175 ± 0.065	0.121 ± 0.041	$0.133 {\pm} 0.024$	0.123 ± 0.038
30	R2	0.913 ± 0.061	0.912 ± 0.060	0.914 ± 0.063	0.907 ± 0.068	0.205 ± 5.614	0.726 ± 0.172	$0.728 {\pm} 0.103$	0.740 ± 0.131
	CC	0.770 ± 0.277	0.766 ± 0.274	0.779 ± 0.269	$0.760 {\pm} 0.284$	0.683 ± 0.270	$0.740 {\pm} 0.261$	0.717 ± 0.246	0.723 ± 0.273
				N	MOVER-SIS				
	MAE	0.026±0.020	0.028±0.016	0.035±0.040	0.031±0.016	0.034±0.041	0.041±0.072	0.044±0.070	0.044 ± 0.074
	RMSE	0.061 ± 0.028	0.061 ± 0.028	0.070 ± 0.047	0.065 ± 0.028	0.086 ± 0.044	0.101 ± 0.074	0.095 ± 0.069	0.097 ± 0.073
1	R2	0.911 ± 0.434	0.926 ± 0.318	0.886 ± 0.632	0.889 ± 0.610	0.902 ± 0.412	0.826 ± 0.925	0.830 ± 0.929	0.823 ± 1.043
	CC	0.914 ± 0.109	0.888 ± 0.147	0.866 ± 0.194	0.879 ± 0.147	0.844 ± 0.226	0.879 ± 0.127	0.896 ± 0.106	0.848 ± 0.211
	MAE	$0.032 {\pm} 0.020$	0.035 ± 0.019	0.038±0.031	0.036 ± 0.018	0.044 ± 0.030	0.047±0.071	0.056±0.068	0.051±0.073
2	RMSE	0.071 ± 0.030	0.071 ± 0.033	0.078 ± 0.040	0.072 ± 0.031	0.105 ± 0.039	0.113 ± 0.071	0.112 ± 0.067	0.114 ± 0.072
3	R2	0.868 ± 0.696	$0.896 {\pm} 0.450$	0.842 ± 0.913	0.855 ± 0.850	0.854 ± 0.633	0.745 ± 1.573	0.751 ± 1.454	0.733 ± 1.692
	CC	0.879 ± 0.143	0.854 ± 0.167	0.841 ± 0.197	0.855 ± 0.165	0.807 ± 0.237	0.854 ± 0.137	$0.836 {\pm} 0.161$	0.821 ± 0.224
	MAE	$0.044 {\pm} 0.023$	0.050 ± 0.024	0.049 ± 0.033	0.046 ± 0.022	0.062 ± 0.029	0.062 ± 0.072	0.081 ± 0.063	0.073 ± 0.061
10	RMSE	0.087 ± 0.034	$0.088 {\pm} 0.039$	0.093 ± 0.043	$0.085{\pm}0.036$	0.138 ± 0.042	$0.144 {\pm} 0.073$	$0.141 {\pm} 0.064$	0.143 ± 0.064
10	R2	0.785 ± 1.303	$0.833 {\pm} 0.740$	0.764 ± 1.422	0.783 ± 1.402	$0.747 {\pm} 1.128$	0.506 ± 3.630	0.576 ± 2.732	0.567 ± 2.966
	CC	$0.820 {\pm} 0.199$	0.769 ± 0.234	0.789 ± 0.225	0.805 ± 0.208	$0.748 {\pm} 0.252$	0.790 ± 0.190	$0.742 {\pm} 0.224$	0.742 ± 0.256
	MAE	0.058 ± 0.027	0.064 ± 0.034	0.061 ± 0.033	$0.056 {\pm} 0.028$	0.091±0.041	0.087 ± 0.067	0.114 ± 0.059	0.098 ± 0.059
30	RMSE	0.101 ± 0.037	0.104 ± 0.050	0.106 ± 0.042	$0.094{\pm}0.041$	0.178 ± 0.055	$0.188 {\pm} 0.078$	0.173 ± 0.064	0.176 ± 0.064
30	R2	$0.658{\pm}2.188$	0.781 ± 0.942	$0.626{\pm}2.428$	0.700 ± 2.011	$0.577 {\pm} 1.924$	-0.125 ± 9.063	$0.321{\pm}4.297$	0.273 ± 4.833
	CC	0.760 ± 0.243	0.699 ± 0.265	0.729 ± 0.272	0.753 ± 0.243	0.661 ± 0.276	0.693 ± 0.245	$0.648 {\pm} 0.257$	0.668 ± 0.270

TABLE X: Full performance comparison of different models on the incomplete variables track. The historical window is set to 30 minutes, and the forecasting horizons are 1, 3, 10, and 30 minutes.

Met	Models	MambaTS (2024)	iTransformer (2023)	FourierGNN (2023)	PatchTST (2023)	Dlinear (2023)	S4 (2022)
				VitalDB			
	MAE	0.020±0.007	0.029±0.008	0.029±0.009	0.026±0.007	0.029±0.007	0.031±0.008
	RMSE	0.040 ± 0.012	0.046 ± 0.012	0.050 ± 0.014	0.052 ± 0.012	0.063 ± 0.014	0.061 ± 0.013
1	R2	$0.946 {\pm} 0.085$	0.928 ± 0.113	0.916 ± 0.142	0.912 ± 0.161	0.874 ± 0.196	0.888 ± 0.171
	CC	$0.930 {\pm} 0.094$	0.923 ± 0.099	0.885 ± 0.134	0.903 ± 0.136	0.902 ± 0.109	0.885 ± 0.144
	MAE	$0.033 {\pm} 0.008$	0.034 ± 0.009	0.034 ± 0.011	0.034 ± 0.009	0.041±0.009	0.039 ± 0.011
,	RMSE	$0.054 {\pm} 0.014$	0.055 ± 0.013	0.057 ± 0.016	0.068 ± 0.016	0.079 ± 0.017	0.076 ± 0.017
3	R2	$0.898 {\pm} 0.182$	0.892 ± 0.193	$0.883 {\pm} 0.228$	0.847 ± 0.316	0.794 ± 0.369	0.802 ± 0.429
	CC	0.869 ± 0.148	$0.877 {\pm} 0.142$	$0.850 {\pm} 0.158$	$0.864 {\pm} 0.152$	$0.850 {\pm} 0.147$	$0.840 {\pm} 0.163$
	MAE	$0.037 {\pm} 0.013$	0.039 ± 0.012	0.042±0.013	0.048 ± 0.013	0.060 ± 0.012	0.055±0.014
10	RMSE	$0.062 {\pm} 0.017$	0.064 ± 0.017	0.067 ± 0.018	0.091 ± 0.022	0.102 ± 0.023	0.098 ± 0.022
10	R2	$0.848 {\pm} 0.339$	$0.839 {\pm} 0.341$	0.821 ± 0.402	0.719 ± 0.510	$0.657 {\pm} 0.561$	0.694 ± 0.499
	CC	$0.822 {\pm} 0.180$	0.800 ± 0.209	0.783 ± 0.214	$0.786 {\pm} 0.195$	0.761 ± 0.202	0.770 ± 0.205
	MAE	$0.047 {\pm} 0.016$	0.050 ± 0.016	0.051±0.016	0.065±0.019	0.082 ± 0.017	0.071 ± 0.022
30	RMSE	0.074 ± 0.021	0.077 ± 0.022	0.077 ± 0.020	0.114 ± 0.032	$0.125{\pm}0.032$	0.119 ± 0.032
30	R2	$0.765 {\pm} 0.495$	0.749 ± 0.507	0.745 ± 0.539	0.569 ± 0.623	0.490 ± 0.661	0.550 ± 0.604
	CC	$0.734 {\pm} 0.250$	0.716 ± 0.275	0.707 ± 0.276	0.689 ± 0.251	0.660 ± 0.252	0.679 ± 0.256
			N	MOVER-SIS			
	MAE	0.032±0.015	0.041±0.022	0.041±0.017	0.038±0.024	0.048±0.029	0.042±0.027
	RMSE	0.079 ± 0.024	0.086 ± 0.032	0.088 ± 0.026	0.092 ± 0.035	0.097 ± 0.035	0.095 ± 0.035
1	R2	$0.901 {\pm} 0.214$	0.890 ± 0.237	0.892 ± 0.211	$0.880 {\pm} 0.225$	$0.868 {\pm} 0.243$	0.873 ± 0.239
	CC	$0.901 {\pm} 0.102$	0.875 ± 0.166	0.875 ± 0.130	0.873 ± 0.154	0.880 ± 0.100	0.866 ± 0.157
	MAE	$0.039 {\pm} 0.017$	0.044 ± 0.023	0.048 ± 0.020	0.048 ± 0.035	0.057 ± 0.035	0.051 ± 0.037
3	RMSE	$0.089 {\pm} 0.025$	0.093 ± 0.030	0.098 ± 0.028	0.107 ± 0.041	0.112 ± 0.039	0.112 ± 0.042
3	R2	$0.874 {\pm} 0.280$	0.863 ± 0.337	$0.864 {\pm} 0.293$	$0.837 {\pm} 0.308$	$0.826{\pm}0.319$	$0.825{\pm}0.328$
	CC	0.872 ± 0.124	0.850 ± 0.175	0.850 ± 0.141	$0.839 {\pm} 0.176$	$0.841 {\pm} 0.127$	$0.831 {\pm} 0.172$
	MAE	$0.052 {\pm} 0.024$	0.055 ± 0.024	0.061±0.025	0.065 ± 0.039	0.079 ± 0.036	0.070 ± 0.042
10	RMSE	$0.105 {\pm} 0.031$	0.108 ± 0.032	0.113 ± 0.033	0.136 ± 0.045	0.137 ± 0.041	$0.142 {\pm} 0.047$
10	R2	$0.818 {\pm} 0.511$	0.802 ± 0.707	0.816 ± 0.411	0.730 ± 0.533	$0.728 {\pm} 0.554$	0.704 ± 0.601
	CC	$0.814 {\pm} 0.170$	0.798 ± 0.198	0.796 ± 0.173	0.771 ± 0.202	0.764 ± 0.174	0.753 ± 0.213
	MAE	$0.068 {\pm} 0.027$	$0.068 {\pm} 0.028$	0.077 ± 0.034	0.090±0.041	0.107 ± 0.037	0.098 ± 0.039
30	RMSE	0.117 ± 0.036	0.120 ± 0.037	0.127 ± 0.041	0.167 ± 0.050	0.161 ± 0.044	0.171 ± 0.047
30	R2	$0.745 {\pm} 0.863$	0.726 ± 1.141	$0.745 {\pm} 0.621$	$0.542{\pm}1.006$	0.578 ± 0.949	0.516 ± 1.122
	CC	0.739 ± 0.229	0.727 ± 0.245	0.711 ± 0.234	0.666 ± 0.245	0.666 ± 0.222	0.644 ± 0.255

TABLE XI: Full performance comparison of different models on the cross-center generalization track. The historical window is set to 30 minutes, and the forecasting horizons are 1, 3, 10, and 30 minutes.

Met	Models	Upper Bound	MambaTS (2024)	iTransformer (2023)	FourierGNN (2023)	PatchTST (2023)	Dlinear (2023)	S4 (2022)
Wict	iles			VitalDB → MC	WED CIC			
	MAE	0.032 ± 0.015	0.035 ± 0.015	0.053 ± 0.024	0.062 ± 0.024	0.042 ± 0.025	0.060 ± 0.028	0.048 ± 0.028
1	RMSE	0.079 ± 0.024	0.083 ± 0.027	0.100 ± 0.034	0.113 ± 0.034	0.098 ± 0.036	0.101 ± 0.032	0.103 ± 0.036
1	R2	0.901 ± 0.214	0.885 ± 0.300	0.839 ± 0.502	0.797 ± 0.524	0.865 ± 0.258	0.853 ± 0.340	0.854 ± 0.265
	CC	0.901 ± 0.102	0.892 ± 0.113	0.850 ± 0.141	0.805 ± 0.174	0.862 ± 0.155	0.864 ± 0.151	0.846 ± 0.164
	MAE	0.039 ± 0.017	0.043 ± 0.018	0.058 ± 0.026	0.061 ± 0.026	0.051 ± 0.037	0.062 ± 0.034	0.054 ± 0.038
3	RMSE	0.089 ± 0.025	0.094 ± 0.029	0.110 ± 0.036	0.116 ± 0.036	0.115 ± 0.043	0.113 ± 0.038	0.117 ± 0.043
	R2	0.874 ± 0.280	0.855 ± 0.351	0.807 ± 0.572	0.789 ± 0.515	0.817 ± 0.327	0.821 ± 0.354	0.813 ± 0.329
	CC	0.872 ± 0.124	0.857 ± 0.146	0.824 ± 0.152	0.794 ± 0.179	0.831 ± 0.160	0.836 ± 0.145	0.821 ± 0.173
	MAE	0.052 ± 0.024	0.056 ± 0.022	0.066 ± 0.026	0.073 ± 0.028	0.068 ± 0.045	0.080 ± 0.036	0.071 ± 0.045
10	RMSE	0.105 ± 0.031	0.111 ± 0.033	0.123 ± 0.038	0.128 ± 0.039	0.145 ± 0.050	0.138 ± 0.041	0.148 ± 0.050
10	R2	0.818 ± 0.511	0.794 ± 0.534	0.745 ± 0.867	0.726 ± 0.795	0.696 ± 0.576	0.721 ± 0.570	0.688 ± 0.574
	CC	0.814 ± 0.170	0.797 ± 0.183	0.764 ± 0.195	$0.734 {\pm} 0.218$	0.758 ± 0.199	0.755 ± 0.191	0.748 ± 0.205
	MAE	$0.068 {\pm} 0.027$	0.071 ± 0.028	0.076 ± 0.031	0.082 ± 0.033	0.093 ± 0.050	0.108 ± 0.038	0.094 ± 0.051
30	RMSE	0.117 ± 0.036	0.125 ± 0.039	0.131 ± 0.041	0.136 ± 0.044	0.181 ± 0.061	0.164 ± 0.045	$0.184{\pm}0.062$
30	R2	$0.745 {\pm} 0.863$	0.715 ± 0.841	0.692 ± 0.954	0.666 ± 0.945	0.472 ± 1.076	0.564 ± 0.974	0.466 ± 1.036
	CC	0.739 ± 0.229	0.717 ± 0.239	0.694 ± 0.246	0.674 ± 0.256	$0.656 {\pm} 0.248$	0.661 ± 0.232	$0.652 {\pm} 0.249$
				MOVER-SIS -	> VitalDB			
	MAE	0.032±0.012	0.033±0.012	0.040±0.011	0.041±0.014	0.038±0.012	0.046±0.011	0.042±0.013
	RMSE	0.059 ± 0.019	0.062 ± 0.018	0.072 ± 0.018	0.071 ± 0.020	0.079 ± 0.019	0.089 ± 0.019	0.083 ± 0.019
1	R2	$0.865{\pm}0.506$	0.827 ± 0.886	0.713 ± 1.919	0.776 ± 1.131	0.618 ± 2.811	0.562 ± 2.922	0.550 ± 3.441
	CC	$0.893 {\pm} 0.104$	$0.893 {\pm} 0.098$	0.874 ± 0.127	0.853 ± 0.144	0.869 ± 0.137	0.862 ± 0.121	0.857 ± 0.148
	MAE	0.039 ± 0.014	0.039 ± 0.014	0.043 ± 0.013	0.046±0.016	0.047±0.014	0.054 ± 0.013	0.050±0.015
2	RMSE	$0.067{\pm}0.020$	0.070 ± 0.020	0.075 ± 0.020	0.078 ± 0.021	0.093 ± 0.022	0.101 ± 0.021	0.098 ± 0.022
3	R2	$0.811 {\pm} 0.767$	0.782 ± 1.001	0.657 ± 2.314	0.717 ± 1.420	0.455 ± 3.894	0.369 ± 4.446	0.342 ± 5.027
	CC	$0.859 {\pm} 0.134$	$0.859 {\pm} 0.126$	0.840 ± 0.158	0.825 ± 0.162	0.830 ± 0.160	0.821 ± 0.149	0.820 ± 0.168
	MAE	0.050 ± 0.018	$0.050 {\pm} 0.018$	0.054 ± 0.016	0.057±0.018	0.063±0.017	0.073±0.016	0.067±0.018
10	RMSE	$0.080 {\pm} 0.024$	0.082 ± 0.024	0.088 ± 0.024	0.090 ± 0.025	0.117 ± 0.027	0.122 ± 0.026	0.123 ± 0.029
10	R2	$0.684{\pm}1.380$	0.666 ± 1.491	0.466 ± 3.705	0.493 ± 3.103	0.325 ± 3.500	0.066 ± 6.455	$0.147{\pm}5.193$
	CC	$0.787 {\pm} 0.190$	$0.787 {\pm} 0.186$	0.767 ± 0.214	0.750 ± 0.221	0.753 ± 0.204	0.737 ± 0.201	$0.736 {\pm} 0.218$
	MAE	$0.062 {\pm} 0.022$	0.063 ± 0.023	0.066±0.021	0.071±0.022	0.084 ± 0.025	0.096±0.023	0.092±0.027
20	RMSE	$0.093 {\pm} 0.029$	0.095 ± 0.030	0.099 ± 0.029	0.104 ± 0.029	0.143 ± 0.037	0.143 ± 0.035	0.146 ± 0.036
30	R2	$0.531{\pm}2.009$	0.523 ± 2.042	0.359 ± 3.825	0.306 ± 4.033	0.020 ± 4.588	-0.205±7.647	-0.085±5.626
	CC	$0.697 {\pm} 0.261$	0.694 ± 0.260	0.680 ± 0.278	0.662 ± 0.282	0.648 ± 0.264	$0.634 {\pm} 0.250$	$0.638 {\pm} 0.265$